THESIS FOR THE DEGREE OF LICENTIATE OF ENGINEERING

in

Thermo and Fluid Dynamics

Assessment and Some Improvements of Hybrid RANS-LES Methods

by

Sebastian Arvidson

Department of Applied Mechanics
CHALMERS UNIVERSITY OF TECHNOLOGY
Göteborg, Sweden, 2013

Assessment and Some Improvements of Hybrid RANS-LES Methods
Sebastian Arvidson

THESIS FOR LICENTIATE OF ENGINEERING no. 2013:01
ISSN 1652-8565

Department of Applied Mechanics
Chalmers University of Technology
SE-412 96 Göteborg
Sweden
Telephone +46-(0)31-7721000

This document was typeset using LaTeX

Printed at Chalmers Reproservice
Göteborg, Sweden, 2013

Assessment and Some Improvements of Hybrid RANS-LES Methods

SEBASTIAN ARVIDSON

sebastian.arvidson@chalmers.se
Department of Applied Mechanics
Chalmers University of Technology

Abstract

Motivated by numerical analysis of a shock/boundary-layer interacting (SBLI) flow in a duct, where some typical existing hybrid RANS-LES methods become awkward to give accurate predictions of the shock-induced corner separation bubble, a new hybrid RANS-LES method, has been proposed. The model is based on a low-Reynolds-number (LRN) $k-\omega$ RANS model, which is one of the few models that are capable of giving reasonable predictions for the SBLI flow in RANS computations.

The proposed hybrid RANS-LES model is not only intended for this specific flow, but also for turbulent flows typically present in aeronautical applications, e.g flow in an air intake or SBLI flow. The model has thus undergone extensive calibration and validation in computations of fundamental flows, namely, Decaying Homogeneous Isotropic Turbulence (DHIT) and channel flows. Ultimately, the proposed model will be further verified in computations of complex aerodynamic flows, such as SBLI and bluff-body flows.

In order to use the same base model in both RANS and LES modes, the LRN effect nestled in the near-wall RANS mode is diminished in the off-wall LES region by a correction function in the proposed model. With this correction function, a weak sensitivity to different grid resolutions is observed for the proposed model in DHIT. The constant C_{LES} was calibrated to 0.70, which is comparable to other hybrid RANS-LES formulations.

In the computation of turbulent channel flow at $Re_\tau = 950$, the RANS-LES interface condition has been evaluated in comparison with available DNS data and different SGS turbulent length scales have been tested. It is suggested that a wall distance based length scale reasonably well supports the turbulence-resolving capability and modeling of near-wall turbulence properties, in comparison with LES using the dynamic Smagorinsky model and the WALE model.

Moreover, the model has been validated further as a zonal approach (similar to embedded LES) in computations of turbulent channel flow at $Re_\tau = 8000$. Different length scales for the LES mode, as well as different RANS-LES switch locations, have been evaluated. It is shown that the wall distance based LES length scale is able to give superior results with a diminishing log-layer mismatch. In general, the model has produced very encouraging predictions of the mean flow and resolved turbulent statistics.

Keywords: hybrid RANS-LES, embedded LES, zonal RANS-LES, PDH-LRN, LES, LES length scale, shock/boundary-layer interaction, log-layer mismatch

Acknowledgements

First of all, I would sincerely like to express my gratitude to my supervisors, Lars Davidson and Shia-Hui Peng, for sharing your knowledge with me. I would like to thank you for giving me the opportunity to explore the field of turbulence modeling and for all the interesting, inspiring and fruitful discussions we have had during the last years. Moreover, I am very thankful for your support and all your positive thinking.

Many thanks to Per Weinerfelt, who has been my supervisor at Saab Aeronautics, for all your help and valuable and constructive discussions about mathematics, CFD solvers, discretization schemes and other things that concern simulations of turbulent flows.

I would like to thank my colleagues at Chalmers, who always contributed to an enjoyable atmosphere. Special thanks to Bastian, with whom I share many nice memories from trips around Europe and Beijing in China. Thanks Ulla and Monica for your guidance through all the administration.

Furthermore, I would like to thank my colleagues at Saab Aeronautics for contributing to a pleasant working environment and for all inspiring discussions about aircrafts, aero-engines and other technical things. I would like to give special thanks to Michael and Sven for having introduced me to the world of propulsion aerodynamics and for being nice and helpful colleagues. Thanks Magnus D., Magnus B. and Hans-Peter, who have given me the opportunity to work as an industrial PhD student and made the engineering work at Saab and the PhD studies into a smooth combination.

A big hug to my father, mother and sister, who are always there for me, support me and encourage me to do this. You are invaluable! Many thanks to my grandmother Bibbi, who is a great supporter. Without your meatballs, muffins and love, this would not have been possible.

Finally, I would like to thank my beloved girlfriend Ann-Charlotte who has encouraged me and given me support in this work.

This work has been funded by the Swedish National Aviation Engineering Research Program (NFFP). I would like to acknowledge the financial support of VINNOVA and Saab Aeronautics. The EU-project ATAAC, in which Saab Aeronautics has been an observer, is also acknowledged. Moreover, the financial support of SNIC (Swedish National Infrastructure for Computing) for computer time at NSC (National Supercomputer Center) and C^{3}SE (Chalmers Center for Computational Science and Engineering) are gratefully acknowledged.

List of publications

This thesis includes the work contained in the following publication:

I Arvidson S., Peng S.-H., and Davidson L. Feasibility of Hybrid RANS-LES of Shock/Boundary-Layer Interaction in a Duct. In Fu S., Haase W., Peng S.-H. and Schwamborn D., editors, *Progress in Hybrid RANS-LES Modelling, NNFM*, volume 117. Springer, 2012.

Contents

Chapter 1

Introduction

With requirements on reduced design costs and developing periods, the importance of model-based design is increasing in today's aero industry. Computational Fluid Dynamics (CFD) plays an important role in the aerodynamic design process and the need for more detailed analysis of complex flows with increased accuracy is growing. Due to the computational resources available today, which are designed for large-scale parallelized computations, the door is opening to advanced flow modeling of unsteady large-scale turbulent phenomena.

With turbulence-resolving flow simulations, which have the possibility to cover flows in a large part of the aircraft's flight envelope, an increased aerodynamic maturity can be reached for the aircraft before wind tunnel tests and flight tests are performed. Test campaigns can be made shorter and less extensive due to the increased maturity of CFD simulation techniques. Thus the cost for designing new aircrafts can be reduced.

The subsections below provide a brief overview of turbulence modeling in general and of turbulence modeling for aeronautical applications. Finally, the scope of this thesis work will be presented.

1.1 Turbulence modeling in general

In principle, the Navier-Stokes equations describe the flow field with all its details. However, since most of the flows around us are turbulent, hence containing a wide range of spatial and temporal scales, it is prohibitively costly to directly solve this set of equations for engineering flows without any assumptions and modeling. Provided flows at low Reynolds numbers, there is still a very limited range of applications in which Direct Numerical Simulations (DNS), i.e. simulations where all turbulent scales are resolved, can be applied.

To achieve affordable computational costs for turbulence-resolving simulations, the resolved turbulent scales must be larger than to those given by DNS. The modeling approaches used today for industrial flows span from Reynolds-Averaged Navier-Stokes (RANS), where all turbulence is modeled, to Large Eddy Simulations (LES),

where only the small scales, called subgrid scales (SGS), are modeled and the large-scale turbulence is resolved.

Spatial filtering is used in LES to separate the resolved turbulence from its modeled counterpart. A flow quantity can thereby be decomposed into a resolved part and a modeled part. The amount of resolved turbulence is determined by the filter width. For finite-volume discretization codes, the filter width is constituted by the local cell size, i.e. a box filter (implicit filtering). For accurate LES predictions, the filter width should be designed so that the cut-off frequency (κ_c) is located in the inertial sub-range, i.e. in the energy spectra where the turbulence is said to be more isotropic and exhibits a $-5/3$-decay. Thus, for wave numbers smaller than κ_c, the turbulence is resolved, and for larger wave numbers, the turbulence is modeled. Since LES resolves the large-scale turbulence, the time step must not be larger than the turbulent fluctuations that are to be resolved.

In RANS, ensemble averaging is used instead of spatial filtering. Compared to time averaging, which is a quantity's mean value over a time interval of a single procedure, ensemble averaging is an average of repeated procedures at a certain time. Ensemble averaging is the reason for keeping the time dependent term in the RANS equations. If time averaging is applied this term is zero. However, in practical flow simulations, ensemble averaging can rarely be used and hence time averaging is applied in practice. Following this argumentation, the RANS equations will in this thesis be referred to as time averaged.

Furthermore, in RANS the flow is decomposed into a mean part and a fluctuating part, which together form the instantaneous quantity. Through this decomposition, all turbulent fluctuations are modeled. Since the unsteady form of RANS (URANS) includes the time-dependent term, it has the ability to capture low frequency unsteadiness, e.g. caused by time dependent boundary conditions or vortex shedding. In URANS, the time step is determined by these low frequency phenomena and is usually much larger than the turbulent time scales, which are all modeled. This is called scale separation. Due to the different time scales resolved in LES and URANS, the time step used in LES simulations has to be much smaller than in URANS.

Independent of whether spatial filtering or time averaging is used, turbulent stresses arise. These must be accounted for with a turbulence model. LES models only the turbulent length scales smaller than $2\pi/\kappa_c$, which are more isotropic. With RANS, the entire energy spectra are modeled, which implies that also the large energy-carrying anisotropic scales must also be modeled.

A wide range of approaches is used in RANS modeling. The simplest models are algebraic and the most sophisticated are Differential Reynolds Stress Models (DRSM), which solve a transport equation for each Reynolds stress. The most common RANS models are however two-equation models, either based on Boussinesq's approximation or with an anisotropy extension to better model anisotropic turbulence, so called Algebraic Reynolds Stress Models. Most commonly in LES, the subgrid-scale models are algebraic to reduce the computational cost. Even though algebraic models based on Boussinesq's approximation involve much less physics than e.g. two equation models, their use is motivated since only the subgrid scale

turbulence is modeled, which is less anisotropic than the larger turbulent scales.

For high Reynolds number wall-bounded flows, RANS remains the favourite choice since it makes the grid-resolution requirement much more relaxed in the wall tangential directions compared to LES. Only the grid in the wall-normal direction has to be fine enough to accurately capture the velocity gradients. A combination of RANS and LES is well suited for efficient flow simulations involving both attached and separated boundary layers at high Reynolds numbers, i.e. hybrid RANS-LES modeling. Hybrid RANS-LES models are a family of different approaches in which RANS and LES are combined, most often through an explicit RANS-LES interface, which is used to separate RANS and LES domains. These methods are further described in Section 2.

However, in the past decade, a number of seamless hybrid RANS-LES methods have been proposed, for example Partially-Average Navier-Stokes (PANS, see e.g. [1]) and Partially-Integrated Transport Method (PITM, see e.g. [2]). These methods are seamless in the sense that no explicit RANS-LES interface is present to distinguish between RANS and LES modes. Both approaches are based on RANS models, which are modified to adapt to a scale resolving model, i.e. LES-like behaviour. Another example of turbulence-resolving modeling is the SAS model (Scale-Adaptive Simulation, see e.g. [3]), which should be seen as an URANS model with scale-resolving capability. The von Kármán length scale, expressed as the quotient of the first-order to second-order derivative of the velocity field, is used as a sensor. Thus, the use of the von Kármán length scale enables the model to induce turbulence-resolving simulations. In PANS, the ratio of modeled to total turbulent kinetic energy (f_k) is used as a sensor to determine whether the model works in turbulence-resolving or RANS mode. The ratio takes values between zero and one, indicating simulations in the range from DNS ($f_k = 0$) to RANS ($f_k = 1$), respectively. In an improved version of the original PANS formulation by Basara et al. [4], the ratio is computed in the simulation and adapted to the flow field. The PANS model has been further extended by Ma et al. [5] to a low Reynolds number formulation. Later in the work by Davidson and Peng [6] an embedded approach using PANS was demonstrated. In this work the ratio of modeled to total turbulent kinetic energy was given as an input to the simulation. Moreover, in the work by Davidson [7], a zonal approach was demonstrated based on PANS, where the near-wall region is treated as RANS and the off-wall region as LES.

1.2 Turbulence modeling for aeronautical applications

A large variation of flows are present in an aircraft's flight envelope: low and high-speed flows, massively separated flows and shallow separations, flows involving shock induced boundary-layer separation, vortex breakdown etc. Aircraft life cycles are extremely long, compared to many other products. Life cycles of 30 years are common for modern aircraft systems. Over such a long life cycle, the aircraft sys-

tem should be fully operational and continually developed. Comparisons between different configurations and flow cases are essential in the development process and thus variations in turbulence models and parameters that can contribute to differences between CFD solutions are avoided. Even though, a large number of RANS turbulence models are available that incorporate different levels of flow physics, eddy-viscosity models are mostly used in the aircraft design process, for example, Spalart-Allmaras one-equation model (SA) [8] and Menter's Shear Stress Transport (SST) $k-\omega$ model (MSST) [9].

Aerodynamic design is often associated with predictions of drag and lift, which are key parameters that are used to predict aircraft performance. These predictions are currently often made using the steady RANS approach. If the flow becomes unsteady, e.g. due to bluff external stores or a high angle of attack, unsteady RANS is applied. It is very seldom that hybrid RANS-LES is applied to a full aircraft configuration, including external stores. These simulations take too long time to perform in the standard design process, even though computer resources have grown significantly over the last decade.

Focusing on propulsion aerodynamics, key parameters are for example total pressure recovery and distortion at the engine face, drag induced by the inlet lips or drag related to the aircraft after-body. In some of these parameters the flow unsteadiness plays an important role, e.g total pressure distortion at the engine face. Prediction of total pressure recovery and drag related to the inlet or the after-body is usually made with RANS, provided that only mild separations are present. However, since the turbulent fluctuations is an important input to the engine stability analysis, the interest for turbulence-resolving methodology has started to grow in propulsion aerodynamics.

Compared to external aerodynamics of a full aircraft, propulsion-aerodynamic related flow problems are easier to isolate from other parts of the aircraft. This makes the applications of turbulence-resolving methods computationally effective to apply. Examples of applications are advanced aerial vehicles, developed for low radar and infrared (IR) signature. These often use bent inlet ducts and outlet nozzles to shield the engine face and turbine outlet from incoming radar or IR-detecting radiation. Such duct configurations tend to increase the turbulence intensity, since they induce swirl and drive the flow towards separation. Moreover, the engine stability is affected by the flow quality at the engine face. Prediction of the flow with high accuracy, including turbulent fluctuations, is therefore essential for a valuable engine stability analysis.

In an even broader perspective, advanced turbulence modeling in flow simulations of full aircraft configurations is not the only key issue. At high wing loads, aero-elasticity may play an important role in obtaining accurate predictions of e.g. the buffeting on a wing. It is not only aerodynamic performance of wings, inlet ducts etc. that are interesting for the whole aircraft system; store separation simulations, which contribute to better knowledge of the aerodynamic interaction between aircraft and payload, are also very valuable, since wind tunnel based store separation tests are costly. Aircraft manoeuvring and flutter are other areas where CFD is ap-

plied to predict aircraft behaviour. Common to all these kinds of simulation is the e.g. the complexity caused by mesh deformation or mesh movement. In some applications, a structural analysis must also be made in the simulation loop to obtain information about geometry deformation.

The use of CFD simulations, and the complexity of aerodynamic problems, have increased over the years. The aeronautical industry is moving towards more advanced turbulence modeling, such as turbulence-resolving methods, in order to accurately predict separated flows. At the same time, the development of methods for simulations, which takes, for example, aero-elasticity and store separation into account, are growing. By combining the abilities of these tracks, model based design in the field of fluid dynamics and aero design, will in the near future form increasingly reliable tools which, to a large extent, can compete with physical testing.

1.3 Scope of this work

This licentiate thesis started with the work presented in the appended paper: *Feasibility of Hybrid RANS-LES Modeling of Shock/Boundary-Layer Interaction in a Rectangular Duct* [10], a flow in a duct that involves shock/boundary-layer interaction and local corner-flow separations. This flow has been shown to be a challenging case in terms of attaining accurate predictions for both conventional RANS models and turbulence-resolving methods. However, it was found that the low-Reynolds-number $k-\omega$ model by Peng et al. [11] (the PDH model) gives results that are in good agreement with experimental data. Since none of the tested turbulence-resolving models in the work was able to produce satisfactory predictions, the main work in this licentiate thesis has been dedicated to the formulation and evaluation of a turbulence-resolving model based on the PDH low Reynolds number $k-\omega$ model.

Even though this work has been motivated by the initial work on the computations using different hybrid RANS-LES models in the transonic duct-flow case, evaluation of the proposed model for this flow case is beyond the scope of this thesis. Instead, the focus is fundamental flows to calibrate and verify the proposed model's turbulence-resolving capability. The proposed model is placed in the category of hybrid RANS-LES methods. In addition, applications are flows at high Reynolds numbers that are typically present in full scale aircraft simulations. Pure LES computations are also included in this work. This is motivated by the study of channel flow using embedded LES, where RANS and LES are combined through a RANS-LES interface located across the channel. As a future step, an embedded LES formulation using the proposed model will be applied to the referred transonic duct-flow case. The studied case of embedded channel flow should therefore be seen as a first step in this direction.

The LES constant has been calibrated in Decaying Homogeneous Isotropic Turbulence (DHIT). To verify the model's capability to capture shear flow, fully developed channel flow at $Re_\tau = 950$ and 8000 was applied. For $Re_\tau = 950$, the model has been used as a full LES model, whereas a zonal hybrid RANS-LES formulation

and a DES formulation have been evaluated for $Re_\tau = 8000$. Moreover, this work sheds light on different LES length scale formulations in an exploration of how the resolving capability is affected.

The thesis is organized as follows. An overview of turbulence modeling and a short description of turbulence modeling for aeronautical applications have been given in this first section. Section 2 gives an overview of hybrid RANS-LES modeling. The idea of hybrid RANS-LES modeling is presented and alternative formulations are discussed. Shortcomings of hybrid RANS-LES are described and approaches to deal with these are presented. The numerical procedures followed to solve the incompressible and compressible Navier-Stokes equations that are utilized in the presented work are presented in Section 3. A new hybrid RANS-LES method based on the PDH low Reynolds number $k-\omega$ model by Peng et al. [11] is formulated in Section 4, whereafter the proposed model is evaluated in Section 5. Simulations of Decaying Homogeneous Isotropic Turbulence and fully developed channel flow have been used for calibration and evaluation. Section 6 gives some concluding remarks together with an outlook of future work.

Chapter 2

Overview of hybrid RANS-LES modeling

Most of hybrid RANS-LES methods use an explicit interface between RANS and LES. These methods can be categorized as: global methods, zonal methods and Wall-Modeled LES (WMLES) methods. This section gives an overview of these hybrid RANS-LES approaches. The idea behind hybrid RANS-LES modeling will be presented, and some typical methods will be highlighted. The aspects and choice of LES length scale formulation will be described and its effect on the model-resolving capability is discussed.

2.1 Idea of hybrid RANS-LES modeling

For hybrid RANS-LES models of a global, zonal and WMLES type, an explicit RANS-LES interface is applied. The intention of these models is to model either the full boundary layer or a part of the boundary layer with RANS and switch to a turbulence-resolving simulation state in off-wall and separated regions. Usually this hybrid RANS-LES modeling adapt a RANS model as a base model and switch to a SGS model by adaption of a turbulent length scale. The chosen length scale lets the hybrid RANS-LES model work in modeling or resolving mode, i.e. RANS or LES, respectively. The length scale used in the LES region, the LES filter width, is commonly defined by the local cell size, Δ, and a model specific constant, C_{DES}. In the literature this constant has different names. For the model based on PDH, which is proposed in this work, it is called C_{LES}. The RANS length scale, or the turbulent length scale, is dependent on the RANS model. For example, the Spalart-Allmaras model [8] uses the wall distance, d, and the turbulent length scale used in Menter's $k-\omega$ SST model [9] is computed from its turbulent quantities, k and ω.

Given the transport equation for the working quantity of the turbulent viscosity for the Spalart and Allmaras model [8] in Eq. 2.1, it can be seen that the turbulent length scale is involved in the destruction term (the last term on the right hand side). By changing d to $C_{DES}\Delta$, i.e. going from RANS to LES, the destruction term will increase since $C_{DES}\Delta < d$ in the off-wall region. An increased destruction of $\widetilde{\nu}_t$

will in turn reduce the level of turbulent viscosity fed into the momentum equations. Provided that the local total stress levels in the flow field have to be kept constant, independent of modeling approach, a reduction of modeled turbulent stresses must be compensated by an increase of the resolved counter parts. Thus, the turbulence has to be resolved and the governing equations work in resolving mode.

$$\frac{D\widetilde{\nu}}{Dt} = c_{b1}\widetilde{S}\widetilde{\nu} + \frac{1}{\sigma}\left[\frac{\partial}{\partial x_j}\left((\nu+\widetilde{\nu})\frac{\partial\widetilde{\nu}}{\partial x_j}\right) + c_{b2}\frac{\partial\widetilde{\nu}}{\partial x_j}\frac{\partial\widetilde{\nu}}{\partial x_j}\right] - c_{w1}f_w\left[\frac{\widetilde{\nu}}{d}\right]^2 \tag{2.1}$$

Yan et al. [12] explore different length-scale substitutions in Wilcox's $k-\omega$ model [13]. Three different formulations were explored. First, the length scale substitution was applied only to the dissipation term in the equation for the turbulent kinetic energy. Second, as the first case, but, in addition, the turbulent viscosity was manipulated to explicitly include the length scale. Third, the length scale substitution was only applied to the turbulent viscosity.

Highlighted in the study was the possibility for the model, in its LES formulation, to reduce to a Smagorinsky model [14]. This means that, under local equilibrium conditions, i.e. when the production balances the dissipation, the turbulent viscosity can be expressed as $\nu_t = (C\Delta)^2 S$, where C is a constant, Δ the filter width and S the strain rate. This is not always obvious and possible. However, the Smagorinsky model is derived using only dimensional analysis, which implies that the model is based on a small amount of physics. Even though the physical basis is weak in this model, it is widely used and performs rather well.

When it is said that the Wilcox $k-\omega$ model, at local equilibrium, can reduce to a Smagorinsky-like turbulent viscosity it only means that the model will not perform worse than the Smagorinsky model. Moreover, if the model cannot reduce to a Smagorinsky-like turbulent viscosity it does not mean that the model is invalid. Thus, for a LES model to be valid, there is no requirement of reducing to a Smagorinsky-like turbulent viscosity.

In formulation one, where both k and ω equations are involved through the turbulent viscosity, local equilibrium has to be satisfied in both equations simultaneously. In RANS mode is this not possible. However, due to the length scale substitution in the dissipation term in LES mode, local equilibrium is satisfied for both equations simultaneously, see further Figure 5.13 where budgets for the hybrid RANS-LES model based on the PDH model are plotted.

Looking at the length-scale substitution, where only the turbulent viscosity is involved (the third formulation), this formulation cannot re-create Smagorinsky's turbulent viscosity, since production and dissipation/destruction do not balance in the k and ω equations simultaneously. For the second formulation, which reduces to a one-equation model for the subgrid-scale turbulent kinetic energy, it is straightforward to show that this model can be expressed in terms of a Smagorinsky turbulent viscosity. Even though all three formulations cannot reduce to a Smagorinsky-like turbulent viscosity, all three formulations give similar results for the computed test case, a NACA0012 profile at an angle of attack of $\alpha = 60°$.

Calibration of the DES constant, which was done using Decaying Homogeneous

Isotropic Turbulence (DHIT), gave quite different results for the different formulations. The lowest value was achieved for the formulation only involving the dissipation term, and the highest value was given for the case where the length scale substitution was applied to both the dissipation term and the turbulent viscosity. The C_{DES} values were in the range of $0.70 - 0.95$. The authors interpreted the differences in C_{DES} values as an indication of the inherent dissipation of the turbulence model formulation, i.e. dissipation of turbulence. A low value of C_{DES} indicates a higher inherent dissipation compared to a formulation given a high C_{DES} value. Moreover, the authors linked the level of inherent dissipation to the term to which the length-scale modification has been applied. Applying the LES length scale only to the dissipation term in the k-equation, i.e. giving the lowest C_{DES} value and the highest inherent model dissipation, only the right part of the energy spectrum is affected. Hence, this change affects the dissipation of turbulence from kinetic energy to heat through the molecular viscosity. As a secondary effect, the subgrid-scale turbulent kinetic energy is decreased, which in turn leads to a lower level of turbulent viscosity. In contrast, when both the destruction term in the k-equation and the turbulent viscosity are changed, the generation of the subgrid-scale turbulent kinetic energy is cut-off at the source since the turbulent viscosity is used to compute the turbulent stresses in the production term. In turn, this gives a more rapid effect on the reduction of turbulent viscosity compared to when only the dissipation term is changed. The authors concluded that the production and destruction terms can be described as having a strong and weak effect, respectively, on the turbulent dissipation.

This refereed study thus shows the importance of using numerical experiments, such as DHIT, for calibrating the turbulence-resolving mode of these models. Therefore, one should not only rely on analytically derived expressions for the DES constant, since those in some cases can be contradictory. As the authors of the study indicated, DHIT is an isolated test case only used for evaluating the pure LES behaviour and not taking any wall effects into account. For these latter effects, fully-developed channel flow can be applied to evaluate the model's capability to capture the log-law, which is as important as accurately capturing the decaying of turbulence according to the energy spectra and the Kolmogorov $-5/3$-law.

Different basic approaches (length scale substitutions) for formulating RANS-LES models exist, and they can be based on different underlying RANS models. Given turbulence-resolving flow without any wall effects, it is obvious that a hybrid RANS-LES model in its LES mode is less sensitive to the base RANS model than to the calibrated C_{DES} value. This shows the importance of DHIT. Other aspects of accurately predicting the resolved turbulence are the discretization scheme used in the solver and the inherent numerical dissipation. Moreover, it can be concluded that the C_{DES} value is dependent to some extent on the code in which the hybrid RANS-LES model is implemented. The importance of high accuracy has clearly been addressed, e.g. during the EU-project ATAAC for simulations of cylinders in cross-flow and vortex breakdown on a delta wing [15]. For wall-bounded flows including non-geometrically defined separations, indeed, the base RANS model plays an im-

portant role. These phenomena are strongly related to the prediction of the near-wall flow, which is taken care of by the RANS mode of the hybrid RANS-LES model. An example is the simulations of the flow over a wall-mounted 2D hump presented in [16], where a more advanced RANS model clearly improves the prediction of the separation and the subsequent recirculation zone.

Since low-frequency turbulent contents are captured by URANS at the RANS-LES interface, only the low-frequency contents are present and the high frequencies are damped by the RANS/URANS mode. Switching from RANS to LES, the grey area, represented by the region where LES mode is applied but the turbulent content is fed in by RANS, is unavoidable and present in most hybrid RANS-LES models [17, 18]. In addition to the fact that it takes a certain distance for the turbulence-resolving content to re-establish due to the absence of high frequency turbulent contents at the interface, high levels of turbulent viscosity are produced in the RANS region and convected across the interface into the LES region. This further delays the formation of three-dimensional turbulent structures and hence also giving rise to the grey-area problem.

2.2 Formulation of the hybrid RANS-LES switch

The first well formulated hybrid RANS-LES model was Detached Eddy Simulation (DES) proposed in 1997 by Spalart et al. [17]. DES was based on the Spalart and Allmaras [8] one-equation turbulence viscosity model but, as mentioned, the formulation of DES may be generalized to any RANS model. DES is a global approach, and the switch between RANS and LES is made by comparing the RANS length scale, l_{turb}, to the LES length scale and choosing the smallest of the two.

$$l_{DES} = \min\left(l_{turb},\ C_{DES}\Delta\right) \tag{2.2}$$

$$\Delta_{max} = \max\left(\Delta_x, \Delta_y, \Delta_z\right) \tag{2.3}$$

Strelets [19] introduced a DES formulation based on Menter's $k-\omega$ SST model [9] by substituting the length scale in the dissipation term in the equation for the turbulent kinetic energy. Through the introduction of the turbulence-resolving mode via Eq. 2.2, the turbulent viscosity is decreased, as in SA-DES, due to the decreased production of k. Contrary to SA-DES, where $l_{turb} = d$, the turbulent length scale in the SST model is based on k and ω, $l_{turb} = k^{1/2}/\left(\beta^*\omega\right)$, and its RANS-LES switch is dependent on the flow field and not only the grid. In its LES mode, l_{turb} is no longer a pure RANS length scale, but a length scale based on the subgrid-scale turbulent kinetic energy and dissipation rate. The expression for the turbulent viscosity in SST-DES is cast in the same formulation as in the RANS model. However, as for the turbulent length scale, k and ω in the turbulent viscosity are now subgrid scale properties, except in the near-wall RANS region.

SA-DES and SST-DES follow the same argumentation that only the destruction/dissipation term is modified. Another approach was proposed by Kok et al. with

their X-LES model [20], which is based on the TNT $k-\omega$ model [21]. As in SST-DES, the dissipation term is modified, but the X-LES formulation of the turbulent viscosity involves a length scale adaption as well. In the RANS region, the turbulent length scale, defined as $l_{turb} = k^{1/2}/\omega$, is used, while Δ is used in the LES region. Due to the introduction of Δ in the subgrid-scale turbulent viscosity, X-LES reduces to a one-equation LES model with the ω-equation decoupled in LES mode.

Since the DES model by Spalart et al. [17], numerous variants and improvements have been reported of hybrid RANS-LES methods. All these are presented with the aim of improving the control of transition from RANS to LES, e.g. using flow-dependent parameters to avoid grid dependent switching. When grid refinement is employed, e.g. in the vicinity of a shock, and Eq. 2.2 is employed, this will affect the interface location between RANS and LES. A refined grid may reduce Δ_{max}, and thus the switch from RANS to LES will be shifted closer to the wall. Compared to SA-DES, where the wall distance is used as the RANS length scale, DES formulations based on e.g. the SST $k-\omega$ model, where l_{turb} depends on k and ω, the subgrid-scale turbulent length scale will reduce due to a reduction of k_{SGS}. Thus, the RANS-LES interface will be shifted closer to the wall, as in SA-DES.

Since the intention of the original S-A DES is to cover the boundary layer in RANS, in order to reduce the computational effort, the grid has to be designed so that the maximum local cell spacing is of the same size as the boundary layer thickness, i.e. $\Delta_{max} \geq \delta$. For complex geometries and thick attached boundary layers, this requirement can hardly be fulfilled, which is regarded as a weakness of the original DES in [17].

When the use of LES mode penetrates into the boundary layer, the turbulent viscosity will decrease and thus the modeled stresses. Even though the mesh is refined locally, as in a shock region or at the trailing edge of a wing, but not fine enough to fulfill the resolution requirements for LES, the resolved stresses are also reduced. This leads to so-called Modeled Stress Depletion (MSD). This is an unfavourable phenomenon, which can lead to premature separation and is refereed to as Grid Induced Separation (GIS) in the literature [22, 23].

Due to the observed MSD and GIS problems, Menter and Kuntz [22] and Spalart et al. [23] proposed new versions of DES, called delayed DES (DDES), with the intention of preventing LES mode from entering the boundary layer. The transition from RANS to LES is delayed by adding a shielding function. The RANS-LES switch is hereby made much less sensitive to grid refinement issues. Since the shielding function also takes the flow properties into account, the switch is able to let the model switch to LES mode if a separated boundary layer is indicated. In line with these global approaches, Deck proposed a zonal DES (ZDES) formulation [24, 25], where RANS and DES zones are prescribed a priori by the user. The motivation for ZDES was that, with adequate knowledge about the flow field, RANS and DES zones can be prescribed to eliminate the risk for MSD and GIS. A similar approach was also demonstrated by Davidson and Peng [26]. Focusing on the delayed DES version presented by Menter and Kuntz, the model uses either of the two switching functions F_1 or F_2 originally from Menter's SST $k-\omega$ model [9]. The model is thus

dedicated to the SST model as a base RANS model. The following expression is used for the delayed DES length scale, where $F_{SST} = F_1$ or F_2, as in [9].

$$l_{DES-CFX} = \min\left(l_{turb}\left(1 - F_{SST}\right), C_{DES}\Delta\right) \tag{2.4}$$

Spalart et al. [23] presented a generalized delaying function, f_d, based on the r-function from the SA model [8], which can be applied to any model involving turbulent viscosity. The principle is similar to the F_1 or F_2 functions, where the basic idea is to use the ratio of the turbulent length scale to the wall distance.

$$r_d = \frac{\nu_t + \nu}{\sqrt{U_{i,j}U_{i,j}}\kappa^2 d_w^2} \tag{2.5}$$

where ν_t and ν are the turbulent and molecular viscosity, respectively, $U_{i,j}$ the derivatives of the velocity field ($\partial u_i/\partial x_j$), κ the von Kármán constant and d_w the wall distance. The value of r_d determines the state of the flow and is used in the delaying/shielding function f_d.

$$f_d = 1 - \tanh\left(\left[C_{d1}r_d\right]^{C_{d2}}\right) \tag{2.6}$$

Constants C_{d1} and C_{d2} are dependent on the base RANS model and must be tuned in order to get a correct shielding of the boundary layer. f_d is designed to take values between 0 and 1, indicating RANS and LES mode, respectively. Compared to the original DES switch in Eq. 2.2, the DDES length scale has a transition zone due to the design of f_d.

$$l_{DDES} = l_{turb} - f_d \max\left(0, l_{turb} - C_{DES}\Delta\right) \tag{2.7}$$

For $f_d = 0$, the RANS length scale l_{turb} is returned. Having $f_d = 1$, the length scale formulation returns the original DES length scale used in LES mode, i.e. Eq. 2.2.

Among the two concepts for delaying the switch from RANS to LES from occurring outside the boundary layer, the formulation of Spalart et al. [23] is the most commonly used today. There are no principle differences between the two variants, except for the generality of Spalart et al.'s formulation. For wall-bounded flows and in contrast to DES, DDES adjusts the thickness of the RANS layer to follow the boundary-layer growth. The treatment of the boundary layer is therefore safer compared to DES, and MSD/GIS is to a large extent avoided. The DDES formulation will however enhance the grey-area problem. A typical example is free shear flow stemming from boundary layers on each side of a flat plate. Provided that DES only covers a part of the flat plate boundary layer in RANS and that DDES covers the full boundary layer, a higher level of turbulent viscosity is convected from the RANS region to the LES region, downstream of the flat plate trailing edge, with DDES. The higher turbulent viscosity delays the formation of turbulence-resolving shear layer instability and thus strongly contributes to the grey area problem. As global hybrid RANS-LES formulations, zonal formulations suffer also from the grey area problem. Contrary to global formulations, zonal formulations make it possible to control the flow across the RANS-LES interface since the interface is a priori known. For example, assume a flow that is transported from a zone where RANS is applied into a zone

which uses LES. The convection and diffusion fluxes of turbulent RANS quantities across the RANS-LES interfaces can in such a case be manipulated to typical SGS levels, thus mitigating the grey area problem [6]. To further speed up the formation of three dimensional turbulent structures and turbulence-resolving flow, synthetic turbulent fluctuations or fluctuations from precursor DNS can be imposed at the interface, as in [6, 27, 28].

Deck recently presented an improved version of ZDES [25]. Instead of only applying RANS and the original DES formulation, the DES zones should be considered as regions where turbulence-resolving formulations can be applied. DES should hence be seen in a broader perspective and also include variants of DES and wall-modeled LES. This makes ZDES much easier to apply to complex geometries. The fact that DDES or WMLES can be applied to regions where separation is a priori unknown makes ZDES come closer to global hybrid RANS-LES formulations, but the zonal formulation is maintained.

Zonal formulations not only invoke domain decompositions where the near-wall flow is treated with RANS and the off-wall flow with LES. In such situations, the main flow is parallel to the RANS-LES interface. Commonly, RANS-LES interfaces are also employed so that the main flow direction is across the interface, for example the embedded LES approaches. The LES region is embedded in surrounding RANS regions. The surrounding zones are coupled, and RANS zones get feedback from the LES zones and vice versa. This has been demonstrated by Deck [24] for a multi-element airfoil and Chauvet et al. [29] for a controlled propulsive jet.

Flow separation can be highly dependent on the incoming boundary layer turbulence, e.g. shallow separations. A formulation such as DDES, where all boundary layer turbulence is treated in RANS, may thus become awkward. As mentioned earlier, boundary layers treated with fully resolved LES are prohibitively costly. Shur et al. [30] proposed Improved DDES (IDDES), a further improvement of DDES [23], with the intention off resolving boundary layer turbulence. IDDES is a global wall-modeled LES approach, where the background RANS model represents the wall modeling part of the LES and is intended to model only the inner part of the boundary layer. Given that the boundary layer has turbulent contents and the mesh resolution is able to resolve the turbulent scales present in the boundary layer, IDDES switches to WMLES mode otherwise, the DDES formulation is retained to treat the boundary layer with RANS. The model is suitable to use in zonal/embedded formulations where turbulent fluctuations are imposed, as IDDES is sensitive to turbulent contents at the inlet boundaries, to reduce the grey-area problem. The hybrid length scale has been reformulated compared to DDES to adapt for the grid resolution and the inlet boundary sensitivity. For further details, see Shur et al. [30]. Moreover, a simplified version of the original IDDES formulation tuned for the MSST model was presented by Gritskevich et al. [31]. This simplified hybrid length scale is presented here.

$$l_{IDDES} = \widetilde{f}_d \cdot l_{turb} + \left(1 - \widetilde{f}_d\right) C_{DES} \Delta_{dw} \tag{2.8}$$

$$\widetilde{f_d} = \max\left[\left(1 - f_{dt}\right), f_b\right] \tag{2.9}$$

$$r_{dt} = \frac{\nu_t}{\sqrt{U_{i,j}U_{i,j}}\kappa^2 d_w^2} \tag{2.10}$$

$$f_b = \min\left[2\exp\left(-9\alpha^2\right), 1.0\right] \tag{2.11}$$

$$\alpha = 0.25 - d_w/\Delta_{max} \tag{2.12}$$

In Eq. 2.15 Δ_{dw} is presented. The RANS length scale l_{turb} is, in general, dependent on the background RANS model. For MSST $l_{turb} = k^{1/2}/\beta^*\omega$. Δ_{max} is according to Eq. 2.3. ν_t is the turbulent viscosity, $U_{i,j}$ the derivatives of the velocity field ($\partial u_i/\partial x_j$), κ the von Kármán constant and d_w the wall distance. f_{dt} is computed as f_d (Eq. 2.6) but where r_d is replaced with r_{dt}.

2.3 Length-scale formulations in LES

The motivation for various length-scale formulations stems from different needs and is dependent on the flow condition considered. It is a fact that the subgrid scale turbulent viscosity is proportional to the square of the length scale. Using different length-scale formulations can thus significantly affect the level of turbulence viscosity produced by the model and hence its capability to resolve turbulence. For hybrid RANS-LES methods, where the intention is to treat parts or the full boundary layer with RANS, a rapid formation of turbulence-resolving flow is essential after the model has switched from RANS to LES. Different aspects of the LES length scale are therefore essential and important to address.

As motivated by Spalart et al. in the formulation of DES [17], Δ_{max} (Eq. 2.3) is chosen in order to protect the boundary layer from LES content and to reduce the risk for MSD/GIS. Moreover, the local maximum cell size is motivated by the fact that the mesh cannot resolve smaller turbulent scales than this measure. Another commonly used length scale, especially in pure LES models, is based on the cubic root of the control volume.

$$\Delta_{vol} = \left(\Delta_x\Delta_y\Delta_z\right)^{1/3} \tag{2.13}$$

Consequently, due to the subgrid-scale turbulent viscosity - filter-width relation, the use of Δ_{max} on stretched grids will produce higher levels of turbulent viscosity compared to Δ_{vol}. This issue was e.g. advocated by Breuer et al. [32] in DES simulations over a flat plate at high incidence. However, using Δ_{vol} was criticized by Spalart [18] for its weak physical interpretation. Davidson and Peng also demonstrated the effect of a different filter width in their zonal formulation [26]. They motivated their choice of the minimum cell size, $\Delta = \min\left(\Delta_x, \Delta_y, \Delta_z\right)$, instead of Δ_{vol} by considerably better performance in channel flow.

For the DES formulation where $\Delta = \Delta_{max}$, the RANS-LES switch is based on a comparison between the wall distance (or any other model-specific turbulent length scale if the SA model is not employed) and the LES length scale. Considering the location of the RANS-LES interface already in the mesh design, the use of a local maximum cell size makes this location much easier to define compared to the location defined by the cubic root of the cell volume. The importance of mesh design for DES applications is further reported in [33].

In off-wall regions and in separated flows, ideally, uniform cells should be used, giving $\Delta_{max} = \Delta_{vol}$. However, in practical engineering flows it is not always possible to form uniform cells, e.g. in plane free shear layers, due to the high computational cost. Given a structured mesh and that $\Delta = \Delta_{max}$, at the trailing edge of the flat plate where the boundary layers emerge and form the free shear layer, the constraint is often set by the span-wise resolution. The stream-wise resolution is adapted to capture the size of the vortices in the xy-plane. Moreover, the resolution in the y-direction is a heritage from the wall normal boundary layer resolution. For plane free shear layers, as highlighted earlier, the grey area problem can be significant due to excessive turbulent viscosity. With free shear layers in mind, Chauvet et al. [29] proposed a length scale based on the direction of the spin axis of the local vorticity. In principal, the length scale is defined by the plane perpendicular to this spin axis of the local vorticity. Thus, the length scale is adapted to the flow field and is only as wide as needed to resolve the local vorticity field, giving a minimum of excess turbulent viscosity.

$$\Delta_\omega = \sqrt{N_x^2 \Delta y \Delta z + N_y^2 \Delta x \Delta z + N_z^2 \Delta x \Delta y} \tag{2.14}$$

$$\boldsymbol{N} = \frac{\boldsymbol{\omega}}{\parallel \boldsymbol{\omega} \parallel}, \quad \boldsymbol{\omega} = \nabla \times \boldsymbol{u}$$

The advantage of using Δ_ω in plane shear flows is shown in [25].

All formulations of the length scale have the purpose of reasonably reducing the subgrid scale turbulent viscosity. Such a reduction also reduces the model's resistance to MSD/GIS. For hybrid RANS-LES applications, modifications of the LES length scale must therefore be made carefully. The DDES approach [23] is based on the maximum cell spacing. To reduce the grey area, Deck [25] proposed a combination of the vorticity based length scale and the local maximum cell size. By using the f_d-function shown in Eq. 2.6, and introducing a threshold value into f_d, Δ_{max} is used below this value and Δ_ω above. Due to the lower turbulent viscosity produced with Δ_ω on stretched grids and because Δ_{max} is not used in the outer part of the boundary layer, the DDES formulation will switch slightly earlier than the original formulation but with a much reduced grey area.

Special attention must be paid to the length scale used in pure LES models or WMLES models, such as the IDDES proposed by Shur et al. [30]. According to Shur et al., not only the cell size should be included in a proper LES length scale for down-to-the-wall integration, but also the wall distance, to include the wall proximity effects. In the very close vicinity of the wall, the flow properties should depend

only on the wall parallel cell measures, while the free flow should return the standard DES length scale in its LES mode, i.e. $\Delta = \Delta_{max}$. In between the two limits, the length scale should depend on the wall distance.

$$\Delta_{dw} = \min\left(\max\left[C_w d_w, C_w \Delta_{max}, \Delta_{nstep}\right], \Delta_{max}\right) \tag{2.15}$$

$C_w = 0.15$, d_w is the wall distance, Δ_{nstep} is the grid-step size in the wall-normal direction and Δ_{max} is according to Eq. 2.3. Shur et al.'s intention with the proposed length scale is to get a smooth reduction of the turbulent viscosity close to the wall with a steep gradient in the off-wall region. This should be compared to a turbulent viscosity based on Δ_{vol}, which has a much steeper growth in the wall-vicinity region with a slower growth in the outer part of the boundary layer.

2.4 Log-layer mismatch

A well known problem in hybrid RANS-LES modeling of attached boundary layers is the log-layer mismatch. The problem is due to unmatched log-layer predictions in the RANS and LES regions, respectively, causing an over predicted velocity in the LES region. In the RANS region, the resolved stresses are weak and the modeled counterpart is strong. Due to the large modeled stress levels, the predicted turbulent length scales at the RANS-LES interface are large and thus a large turbulent viscosity is given. In the LES region, the stresses should be dominated by their resolved part. Ideally, the resolved stresses should be fully developed at the RANS-LES interface and the modeled stresses should be reduced to typical subgrid-scale levels. However, the high turbulent viscosity from the RANS region is transported across the interface into the LES region, acting to delay the development of turbulence resolving flow. An unphysical buffer region (sometimes refereed to as a super-buffer region [34]), similar to the grey area problem, is therefore created.

The stresses have to be balanced on each side of the RANS-LES interface. Due to the limited level of resolved stresses, on the LES side, close to the interface, the modeled and viscous parts of the stresses in the LES region are over-predicted in order to compensate for the under predicted resolved part. Since the modeled and viscous stresses are proportional to the velocity gradients, the under resolved flow consequently results in increased velocity gradients. The velocity is over-predicted and a reduction in skin friction is achieved.

In aero applications where the boundary layer prediction is essential to accurately predicting drag and separations, the log-layer mismatch has to be reduced as much as possible. The idea of DES is, as mentioned earlier, to model the entire boundary layer in RANS and not be used as a wall-modeled LES. The distinction between DES and wall-modeled LES was discussed by Spalart et al. [23] with their proposed delayed DES. Using DES or hybrid RANS-LES modeling as wall-modeled LES, where the RANS model acts as the wall model, has however been studied e.g. by Nikitin et al. [34] and Davidson and Peng [26]. Attempts to reduce the log-layer mismatch in such applications have been presented by e.g. Davidson and Billson

[27] and Davidson and Dahlström [35], where turbulent fluctuations are imposed at the RANS-LES interface to stimulate the development of turbulence resolving flow and reduce the over prediction of modeled and viscous stresses in the LES region. Another attempt to reduce the log-layer mismatch is the improved delayed DES proposed by Shur et al. [30]. They formulated a new LES length scale, adapted for attached boundary layers, and introduced a set of blending functions.

Chapter 3

Numerical method

Two different solvers have been used in this thesis; one incompressible and one compressible. The incompressible solver was used in the DHIT simulations presented as well as in the simulations of fully developed channel flow and channel flow using embedded LES. The compressible solver has been applied to the transonic duct flow case presented in Arvidson et al. [10].

3.1 Incompressible flow

Since zonal, embedded and DES formulations of the proposed model are examined, both unsteady RANS and LES are applied in the same domain. The modeling mode, i.e. RANS or LES, determines whether the Navier-Stokes equations are either time averaged or spatially filtered. The solver used is based on a finite volume technique; the spatial filter width is therefore constituted by the local cell size, Δ. In the following equations, the bar $(\bar{\cdot})$ indicates time averaging or spatial filtering of a quantity. Time averaging of an arbitrary quantity is given as follows:

$$\overline{\Phi} = \lim_{T\to\infty} \frac{1}{T} \int_{-T/2}^{T/2} \Phi dt, \qquad \Phi = \overline{\Phi} + \Phi' \tag{3.1}$$

where Φ' denotes the fluctuating part of Φ. Spatial filtering of an arbitrary quantity, here using a 1D filter for simplification, reads:

$$\overline{\Phi}\left(x,t\right) = \frac{1}{\Delta x} \int_{x-0.5\Delta x}^{x+0.5\Delta x} \Phi\left(\xi,t\right) d\xi, \qquad \Phi = \overline{\Phi} + \Phi'' \tag{3.2}$$

where Φ'' denotes the modeled part of Φ. However, all simulations presented are three-dimensional, a three-dimensional spatial filter was used. Since heat transfer was not of interest for the flow problems analyzed, constant density was applied in all simulations. The continuity and momentum equations, where time averaging or spatial filtering has been applied, reads

$$\frac{\partial \overline{u}_i}{\partial x_i} = 0 \tag{3.3}$$

$$\frac{\partial \overline{u}_i}{\partial t} + \frac{\partial \left(\overline{u}_i \overline{u}_j\right)}{\partial x_j} = -\frac{1}{\rho}\frac{\partial \overline{p}}{\partial x_i} + \frac{\partial}{\partial x_j}\left(\nu \frac{\partial \overline{u}_i}{\partial x_j} - \tau_{ij}\right) \tag{3.4}$$

where $\tau_{ij} = \overline{u_i u_j} - \overline{u}_i \overline{u}_j$ denotes the subgrid scale turbulent stresses, which need to be modeled. Due to the different modeling modes, i.e. RANS or LES, the turbulent viscosity (μ_t) is either a RANS or a subgrid-scale property.

In the simulations of fully developed channel flow, the term $\beta\delta_{1i}$, representing the driving pressure gradient ($\beta = 1$), is added on the right hand side of the momentum equations in order to balance the channel wall shear stress.

The solver used offers different spatial discretization schemes; central differencing, van Leer and a hybrid scheme. Different schemes were applied depending on the application. The discretization scheme used is specified in each test-case section. The temporal advancement is made with the second order Crank-Nicolson scheme. An implicit, fractional step technique with a multigrid Poisson solver [36] was used on a non-staggered grid arrangement. For a more detailed description of the numerical procedure, see Davidson and Peng [26].

3.2 Compressible flow

The unstructured solver Edge [37] was used in this thesis to solve the compressible Navier-Stokes equations. For steady state problems, Edge uses an explicit three-stage Runge-Kutta scheme with the aid of an agglomerated multi-grid and residual smoothing for convergence acceleration. For unsteady simulations, a dual time-stepping approach is applied, combining the Runge-Kutta method with an implicit second-order scheme for physical time advancement. A second order central differencing scheme has been used for the spatial discretization of the momentum equations and the turbulent transport equations.

As for the incompressible solver, time averaging or spatial filtering of the equations are done depending on whether RANS or LES is applied. The Edge solver is, as the incompressible solver, a finite volume based solver and uses the box filter. When applying either time averaging or the spatial filter, as used in the incompressible solver described above, to the compressible Navier-Stokes equations, fluctuating components of the density will arise. To avoid this and get filtered equations similar to the corresponding unfiltered equations, the Favre filter, i.e. a mass-weighted spatial filter, is used for the velocity, temperature and energy components. Spatial filtering or time averaging, as described in Eq. 3.1 and 3.2, are applied to the density and the pressure components. Moreover, if a spatial filter is used where density fluctuations are present, more complicated subgrid-scale terms would appear which need modeling. The decomposition and how a Favre filtered quantity is related to the spatially filtered quantity is expressed as follows:

$$\widetilde{\Phi} = \frac{\overline{\rho\Phi}}{\overline{\rho}}, \qquad \Phi = \widetilde{\Phi} + \Phi'' \tag{3.5}$$

The set of equations solved in Edge, where $(\bar{\cdot})$ denotes time averaging or spatial filtering and $(\tilde{\cdot})$ denotes Favre filtering, are summarized.

$$\frac{\partial \overline{\rho}}{\partial t} + \frac{\partial \left(\overline{\rho}\widetilde{u}_i\right)}{\partial x_i} = 0, \tag{3.6}$$

$$\frac{\partial \left(\overline{\rho}\widetilde{u}_i\right)}{\partial t} + \frac{\partial \left(\overline{\rho}\widetilde{u}_i\widetilde{u}_j\right)}{\partial x_j} = -\frac{\partial \overline{p^*}}{\partial x_i} + \frac{\partial}{\partial x_j}\left[\left(\mu + \mu_t\right)\frac{\partial \widetilde{u}_i}{\partial x_j}\right] \tag{3.7}$$

$$\frac{\partial \left(\overline{\rho}\widetilde{e}_0\right)}{\partial t} + \frac{\partial \left(\overline{\rho}\widetilde{e}_0\widetilde{u}_j\right)}{\partial x_j} = -\frac{\partial \overline{p^*}\widetilde{u}_j}{\partial x_j} + \frac{\partial}{\partial x_j}\left[q_j + \widetilde{u}_i\tau_{ij} + \left(\mu + \frac{\mu_t}{\sigma_k}\right)\frac{\partial k}{\partial x_j}\right] \tag{3.8}$$

where k is the turbulent kinetic energy defined as:

$$k = \frac{1}{2}\widetilde{u_i'' u_i''} \tag{3.9}$$

p^* and e_0 are the static pressure and the total internal energy, both containing the turbulent kinetic energy.

$$\overline{p}^* = \overline{p} + \frac{2}{3}\overline{\rho}k \tag{3.10}$$

$$\widetilde{e}_0 = \widetilde{e} + \frac{1}{2}\widetilde{u}_k\widetilde{u}_k + k \tag{3.11}$$

where $\widetilde{e}$ is the internal energy. The stresses are computed as:

$$\tau_{ij} = \left(\mu + \mu_t\right)\left[2\widetilde{S}_{ij} - \frac{2}{3}\widetilde{S}_{kk}\delta_{ij}\right] \tag{3.12}$$

where $\widetilde{S}_{ij}$ is the Favre filtered strain-rate tensor.

$$\widetilde{S}_{ij} = \frac{1}{2}\left(\frac{\partial \widetilde{u}_i}{\partial x_j} + \frac{\partial \widetilde{u}_j}{\partial x_i}\right) \tag{3.13}$$

To compute the heat fluxes, Fourier's heat law is applied.

$$q_j = \left(\kappa + \kappa_t\right)\frac{\partial \widetilde{T}}{\partial x_j}, \quad \kappa = c_p\frac{\mu}{Pr}, \quad \kappa_t = c_p\frac{\mu_t}{Pr_t} \tag{3.14}$$

Chapter 4

Improved hybrid RANS-LES modeling

4.1 Motivation of the base RANS model

The Low-Reynolds-Number $k-\omega$ model by Peng et al. [11] (PDH-LRN) was recently used in transonic duct flow and produced good results [10]. The reported flow case involves shock/boundary-layer interaction (SBLI) and local recirculation zones in the rectangular duct corners at the shock. The study made a comparison of several models, including RANS models as well as turbulence-resolving approaches. Most of the models had problem in accurately predicting the onset of the separation bubble caused by the shock, due to an inaccurately predicted incoming boundary layer. It was concluded that the near-wall modeling is essential for the studied flow case, due to the SBLI phenomenon, as well as the prediction of local recirculation bubbles. Among the models used in the study, PDH-LRN was the only model that is able to appropriately represent the flow field.

Taking a step towards improved hybrid RANS-LES modeling, the PDH-LRN model is thus selected as the base RANS model for the reported flow case. Moreover, one of the purposes of this thesis is to find a suitable RANS base model for internal flows where local and shallow separation occurs. The fact that the PDH-LRN model is designed and intended for internal flows with local separations is desirable in order to use it as a background model in hybrid RANS-LES modeling.

Along with a recalibration of model constants and damping functions, different from the Wilcox's low-Reynolds-number model [38], an additional turbulent cross-diffusional term is added in the ω-equation in the PDH-LRN model. Contrary to Menter's BSL and SST models [9], the cross-diffusion term in PDH-LRN is active in the near-wall region. Close to the wall, the derivatives of k and ω are often of opposite signs, giving that the cross-diffusion term sometimes acts as a sink term. In the near-wall region, k is thus increased due to the reduction of ω and, in turn, an increased turbulent viscosity is achieved. The model constants are recalibrated compared to Wilcox's LRN model and the near-wall damping functions are reconstructed to allow for correct asymptotic near-wall behaviour. The transport equations and the

turbulent viscosity for the PDH-LRN $k-\omega$ model are summarized.

$$\frac{D\rho k}{Dt} = \tau_{ij}\frac{\partial u_i}{\partial x_j} - D^k + \frac{\partial}{\partial x_j}\left[\left(\mu + \frac{\mu_t}{\sigma_k}\right)\frac{\partial k}{\partial x_j}\right] \tag{4.1}$$

$$\begin{aligned}\frac{D\rho\omega}{Dt} &= C_{\omega_1} f_\omega \frac{\omega}{k}\tau_{ij}\frac{\partial u_i}{\partial x_j} - C_{\omega 2}\rho\omega^2 \\ &+ \frac{\partial}{\partial x_j}\left[\left(\mu + \frac{\mu_t}{\sigma_\omega}\right)\frac{\partial \omega}{\partial x_j}\right] + C_\omega \frac{\mu_t}{k}\frac{\partial k}{\partial x_j}\frac{\partial \omega}{\partial x_j}\end{aligned} \tag{4.2}$$

$$\mu_t = C_\mu f_\mu \frac{\rho k}{\omega} \tag{4.3}$$

D/Dt on the left hand side of the transport equations is the material derivative; $D/Dt = \partial/\partial t + u_i \partial/\partial x_i$. As a further adaption to complex internal flows, the only governing parameter used in the damping functions f_k, f_ω and f_μ, is the turbulent Reynolds number, Eq. 4.7. Compared to any wall distance related quantity, which can be an ambiguous quantity for complex internal flows, the turbulent Reynolds number is well defined since no geometrical properties are involved. On the other hand, in a LES and hybrid RANS-LES perspective, the wall distance has been shown to be a suitable parameter to involve in the formulation of the LES length scale [30]. Thus, in turbulence-resolving simulations, the inclusion of the wall distance might be needed, even though this quantity is not involved in the low-Reynolds-number damping functions.

$$f_k = 1 - 0.722 \cdot \exp\left[-\left(\frac{R_t}{10}\right)^4\right] \tag{4.4}$$

$$f_\omega = 1 + 4.3 \cdot \exp\left[-\left(\frac{R_t}{1.5}\right)^{1/2}\right] \tag{4.5}$$

$$\begin{aligned}f_\mu = 0.025 &+ \left\{1 - \exp\left[-\left(\frac{R_t}{10}\right)^{3/4}\right]\right\} \\ &\left\{0.975 + \frac{0.001}{R_t}\cdot\exp\left[-\left(\frac{R_t}{200}\right)^2\right]\right\}.\end{aligned} \tag{4.6}$$

The turbulent Reynolds number is defined as:

$$R_t = \frac{k}{\nu\omega} \tag{4.7}$$

Finally, the closure constants for the PDH-LRN model are presented.

$$\sigma_k = 0.8 \quad \sigma_w = 1.35 \quad C_\mu = 1.0 \quad C_k = 0.09$$
$$C_{\omega 1} = 0.42 \quad C_{\omega 2} = 0.075 \quad C_\omega = 0.75$$

4.2 Formulation of the turbulence-resolving mode

As highlighted in Section 2, there is no obvious choice of how to formulate a hybrid RANS-LES model from an existing RANS model. There are several length scale substitutions to choose from, and they all have their advantages and downsides. However, to keep the ω-equation involved in the subgrid-scale formulation in the proposed model also, only the dissipation term in the k-equation is modified, in accordance with Strelets SST-DES [19]. The turbulent length scale, expressed in k and ω, is substituted in the dissipation term, which gives the possibility to formulate the hybrid RANS-LES model.

$$D^k = C_k f_k \rho k \omega = \rho f_k \frac{k^{3/2}}{l_{turb}} \tag{4.8}$$

The turbulent length scale is chosen according to the modeling mode, i.e. $l_{turb} = l_{RANS}$ or $l_{turb} = l_{LES}$.

$$l_{RANS} = \frac{k^{1/2}}{C_k \omega} \tag{4.9}$$

$$l_{LES} = \Psi_{PDH} C_{LES} \Delta \tag{4.10}$$

With $l_{turb} = l_{RANS}$, the original PDH-LRN model is returned. When $l_{turb} = \Psi_{PDH} C_{LES} \Delta$, the LES mode of the proposed hybrid RANS-LES model is achieved. Δ is the LES length scale and $C_{LES} = 0.70$ was calibrated using decaying homogeneous isotropic turbulence (DHIT). These results are presented in more detail in Section 5. Since the PDH-LRN model uses low Reynolds number damping functions, the correction function, Ψ_{PDH}, is added to the LES formulation as recommended by Spalart et al. [23]. Modeling constants and damping functions in the proposed model are according to the PDH-LRN model [11].

Contrary to RANS models where all turbulence is modeled, only the subgrid-scale turbulence is modeled in LES. Thus, the local turbulent Reynolds numbers reach much lower levels as compared to RANS, which can make the damping functions activated even though the flow is detached and when walls are far away. Since the amount of modeled turbulence is dependent of the grid resolution, the local turbulent Reynolds number and the turbulent viscosity are dependent of the grid resolution as well. Moreover, the amount of damping achieved by the damping functions is hence dependent on the grid resolution, a dependency which has to be avoided. The purpose of the correction function, Ψ_{PDH}, is thus to eliminate the low-Reynolds-number damping made by the damping functions in the off-wall LES region and keep them in the RANS region. At local equilibrium, the introduction of Ψ_{PDH} is equal to deactivating the damping functions in LES mode. However, the damping functions should be used when RANS is applied. Through the introduction of the correction function in the LES length scale, the same set of model constants/equations can thus be used in the whole flow domain. The correction function will now be derived for the PDH-LRN model in accordance with the work of Mockett [39].

A generalized form of the Smagorinsky turbulent viscosity can be formulated in a PDH-LRN framework using the function A_{PDH} and the correction function Ψ_{PDH}.

$$\nu_t = A_{PDH} \left(\Psi_{PDH} C_{LES} \Delta\right)^2 S \tag{4.11}$$

To return the original formulation of the Smagorinsky turbulent viscosity, the correction function should cancel the low-Reynolds-number dependency of A_{PDH}, i.e. $A_{PDH}\Psi_{PDH}^2 =$ const. Assume that the proposed model is in LES mode (away from the wall) and that the turbulent transport equations are in local equilibrium, i.e. when production and dissipation/destruction balance in the k and ω equations. Note that in a RANS framework, the k and ω equations cannot be in local equilibrium simultaneously. However, due to the introduction of the turbulence resolving mode through the dissipation term in the k-equation, an extra degree of freedom is given to the turbulent transport equations, and local equilibrium can be simultaneously fulfilled away from the wall (see Section 5). The k and ω equations in LES mode at local equilibrium are expressed.

$$\nu_t S^2 = f_k \frac{k^{3/2}}{\Psi_{PDH} C_{LES} \Delta} \tag{4.12}$$

$$\nu_t S^2 = \frac{C_{\omega 2}}{C_{\omega 1}} \frac{1}{f_\omega} \omega k \tag{4.13}$$

The turbulent viscosity, as expressed in Eq. 4.3, can be used to get an expression for the dissipation rate.

$$\nu_t = C_\mu f_\mu \frac{k}{\omega} \quad \Longrightarrow \quad \omega = C_\mu f_\mu \frac{k}{\nu_t} \tag{4.14}$$

The subgrid-scale turbulent kinetic energy can be expressed by combining Eq. 4.13 and 4.14.

$$k = \sqrt{\frac{C_{\omega 1}}{C_{\omega 2}} \frac{f_\omega}{C_\mu f_\mu}} \nu_t S \tag{4.15}$$

Putting Eq. 4.15 in 4.12 can form an expression for the PDH-LRN Smagorinsky-like turbulent viscosity.

$$\nu_t = \frac{1}{f_k^2} \left(\frac{C_{\omega 2}}{C_{\omega 1}} \frac{C_\mu f_\mu}{f_\omega} \right)^{3/2} \left(\Psi_{PDH} C_{LES} \Delta\right)^2 S \tag{4.16}$$

Recapitulate Eq. 4.11 and identify the terms in Eq. 4.16. The expression for the function A_{PDH} can hence be written.

$$A_{PDH} = \frac{1}{f_k^2} \left(\frac{C_{\omega 2}}{C_{\omega 1}} \frac{C_\mu f_\mu}{f_\omega} \right)^{3/2} \tag{4.17}$$

As seen, A_{PDH} depends on the damping functions, which in turn are functions of the local turbulent Reynolds number. To achieve $A_{PDH}\Psi_{PDH}^2 = const$, A_{PDH}^* is introduced in order to represent A_{PDH} when $R_t \to \infty$.

$$R_t \to \infty \Longrightarrow f_k,\ f_\omega,\ f_\mu \to 1$$

$$A_{PDH}^* = \left(\frac{C_{\omega 2} C_\mu}{C_{\omega 1}}\right)^{3/2} \tag{4.18}$$

In correspondence with A_{PDH}^*, we seek a function $\Psi_{PDH}^* = 1$, i.e. Ψ_{PDH} when $R_t \to \infty$. The formulation of the correction function, including numerical limiters, can now be outlined.

$$\left(\frac{\Psi}{\Psi^*}\right)^2 = \frac{A^*}{A} \quad \Longrightarrow \quad \Psi_{PDH} = \min\left[10, f_k\left(\frac{f_\omega}{f_\mu}\right)^{3/4}\right] \tag{4.19}$$

The upper limit of Ψ is chosen according to Spalart et al. [23]. The damping functions and the derived correction function are plotted in Figure 4.1 as a function of the turbulent Reynolds number.

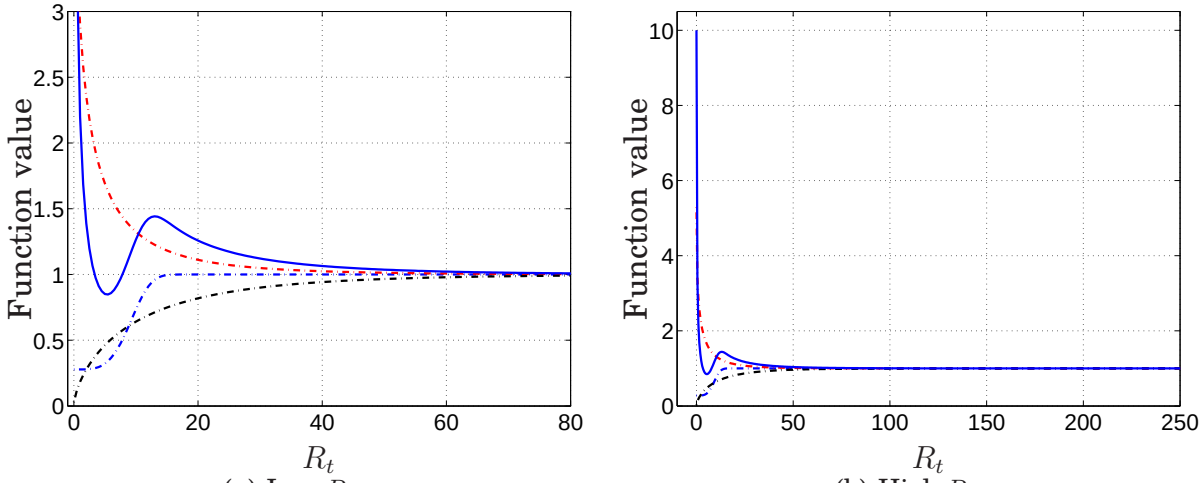

(a) Low R_t. (b) High R_t.

Figure 4.1: Damping functions and correction function used in PDH-LRN. - - - : f_k; - · - : f_ω; - - - : f_μ; —— : Ψ_{PDH}.

Chapter 5

Calibration and evaluation of the modeling approach

As a first step in the development of the turbulence-resolving model using the PDH-LRN as a base model, three test cases have been computed; Decaying Homogeneous Isotropic Turbulence (DHIT), fully developed channel flow and channel flow using embedded LES. In fully developed channel flow, the proposed model has been evaluated for $Re_\tau = 950$ and $Re_\tau = 8000$. For the two Reynolds numbers, the pure LES and hybrid RANS-LES formulations have been applied, respectively. A Reynolds number of $Re_\tau = 950$ was used for the embedded channel flow case.

A description of the test cases follows. The computational mesh characteristics and any specific numerical settings for the test cases will be described. The purpose of the test cases are motivated and, if any specific model settings have been used, these will be presented in each test case section.

5.1 Decaying Homogeneous Isotropic Turbulence

The turbulence-resolving mode of the proposed hybrid RANS-LES model was calibrated using Decaying Homogeneous Isotropic Turbulence (DHIT). This standard test case, used for calibrating turbulence-resolving methods, aims at determining the value of C_{LES}. The constant is chosen so that the resolved turbulence decays according to the energy spectra measured from decaying grid turbulence. In this study, experimental benchmark data by Comte-Bellot and Corrsin [40] have been used for comparison.

To investigate the effect of grid density on C_{LES}, DHIT was computed on two grids. Each grid, with a domain size of $(2\pi)^3$, consisted of 32^3 and 64^3 cubic shaped cells, respectively. For each grid, the test case was computed both with and without the correction function, Ψ_{PDH}, activated. On the 64^3 grid, a simulation was also made where the correction function was excluded and the damping functions were set to 1 to verify a correct behaviour of Ψ_{PDH}. Periodic boundary conditions were applied in all directions and the simulation was initiated with a prescribed velocity field with zero mean velocity. To reach adequate start values for k and ω (turbu-

lent viscosity), 4000 iterations were computed with a frozen velocity field, which was used as an initial condition for the unsteady DHIT simulation. In each time step, 20 sub-iterations were needed to get a well converged solution. The time step was set to $\Delta t = 5 \cdot 10^{-3}\ s$. Energy spectra and the initial velocity fields were generated by a widely used computer program from the group of Professor Strelets in St. Petersburg. Spectra are presented at two non-dimensional time steps; $T = 0.87$ and 2.0, respectively.

The used criteria for selecting the best suited C_{LES}-value is according to Bunge [41]. In short this means; the 32^3 grid is prioritized over the 64^3 grid. The 32^3 gird is seen as more representative for grids used in practical DES simulations of complex geometries/flows. Furthermore, $T = 2$ has precedence over $T = 0.87$.

Energy spectra from DHIT simulations, using the turbulence-resolving mode of PDH-LRN, are presented in Figures 5.1 and 5.2. On the coarse grid, the proposed model was calibrated with and without the correction function, giving $C_{LES} = 0.70$ and 0.95, respectively. As seen in Figure 5.1, the results are identical. Using $C_{LES} = 0.70$, but including the damping functions activated without the correction function, the decay of turbulence is too weak. Compared to the simulations on the finer 64^3 grid shown in Figure 5.2, $C_{LES} = 0.95$ gives too strong a decay compared to experimental data. Comparing the two simulations where the damping functions were set to 1 and the other with Ψ_{PDH} active on the fine mesh, an identical decay of turbulence is achieved, which shows an adequate behaviour of the correction function. For higher wave numbers (κ), as observed on the finer grid, the decay is slightly overpredicted, even though the correction function is activated.

The simulations presented in Figures 5.1 and 5.2, show, according to the selection criteria, that $C_{LES} = 0.70$ is a representative value for the proposed model. This value is in line with other well known base RANS models used for hybrid RANS-LES modeling, as shown in Table 5.1.

In engineering applications, a grid density corresponding to the coarse mesh is often more representative than the finer grid. The stronger influence of Ψ_{PDH} seen on the coarse grid thus motivates its use, even though the influence of the low Reynolds number correction function is weak on the 64^3 grid.

Table 5.1: Constant calibrated in DHIT for different hybrid RANS-LES models.

Base model	C_{DES} or C_{LES}	LRN correction
SA	0.65	No[a]
MSST	0.61, 0.78	No
PDH-LRN	0.70	Yes

[a]The original SA-DES does not include any low Reynolds number correction, but one is proposed in [23].

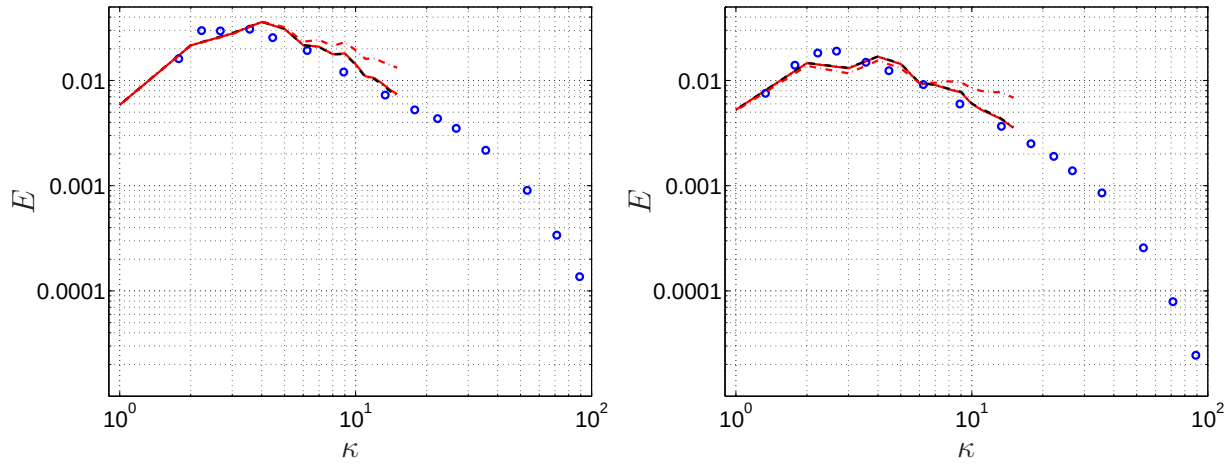

(a) $T = 0.87$ (b) $T = 2$

Figure 5.1: Energy spectra from DHIT using PDH on a 32^3 cell grid. —: Ψ active ($C_{LES} = 0.70$); - - -: no Ψ_{PDH} ($C_{LES} = 0.70$); - · -: no Ψ ($C_{LES} = 0.95$). ○: Experiments [40].

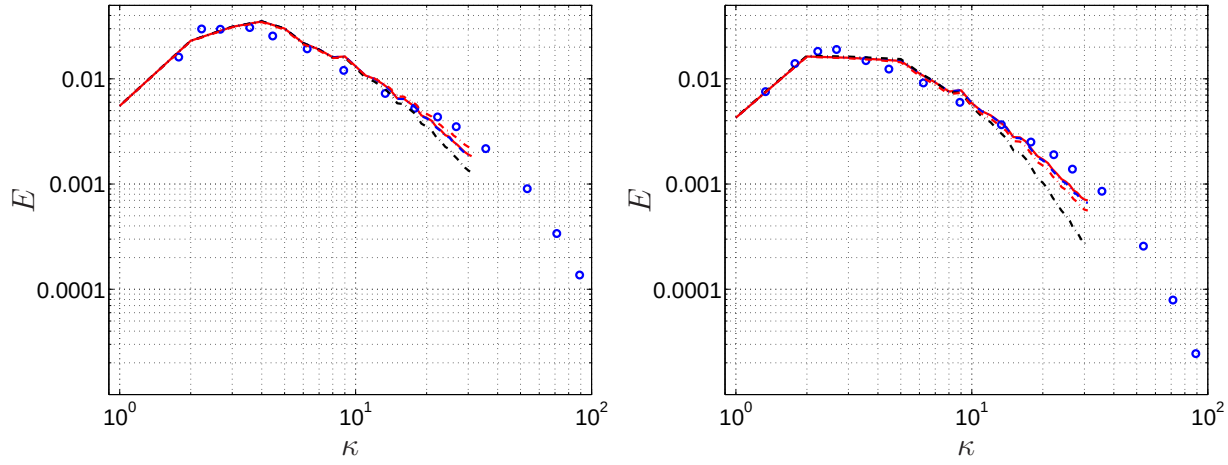

(a) $T = 0.87$ (b) $T = 2$

Figure 5.2: Energy spectra from DHIT using PDH-LRN on a 64^3 cell grid. —: Ψ active ($C_{LES} = 0.70$); - - -: no Ψ_{PDH} ($C_{LES} = 0.70$); - · -: no Ψ ($C_{LES} = 0.95$); - - -: no damping functions ($C_{LES} = 0.70$). ○: Experiments [40].

The time history of the turbulent viscosity together with the turbulent Reynolds number, turbulent kinetic energy and the model functions are presented for both grids used in Figures 5.3 and 5.4. It is clear that the local turbulent Reynolds numbers in both simulations are low enough to activate the damping functions, giving a non-unity value of the correction function, Ψ_{PDH}. Recapitulating Figure 4.1, the limit where the low Reynolds number damping is negligible is $R_t > 80$. Hence, the

turbulent Reynolds numbers given by the DHIT simulations presented are far lower than $R_t = 80$, which further motivates the use of Ψ_{PDH}. The spectra show that the sensitivity to C_{LES} is enhanced on the coarse grid. The influence of the model is stronger on this grid since higher turbulent viscosity levels are produced and lower amounts of resolved turbulent kinetic energy are achieved compared to the fine grid, as seen in Figure 5.4. Theoretically, the production and dissipation in the k-equation should be equal on both meshes. According to Eq. 4.1, this gives that k_{sgs} should also be equal on both meshes, which is seen in Figure 5.4.

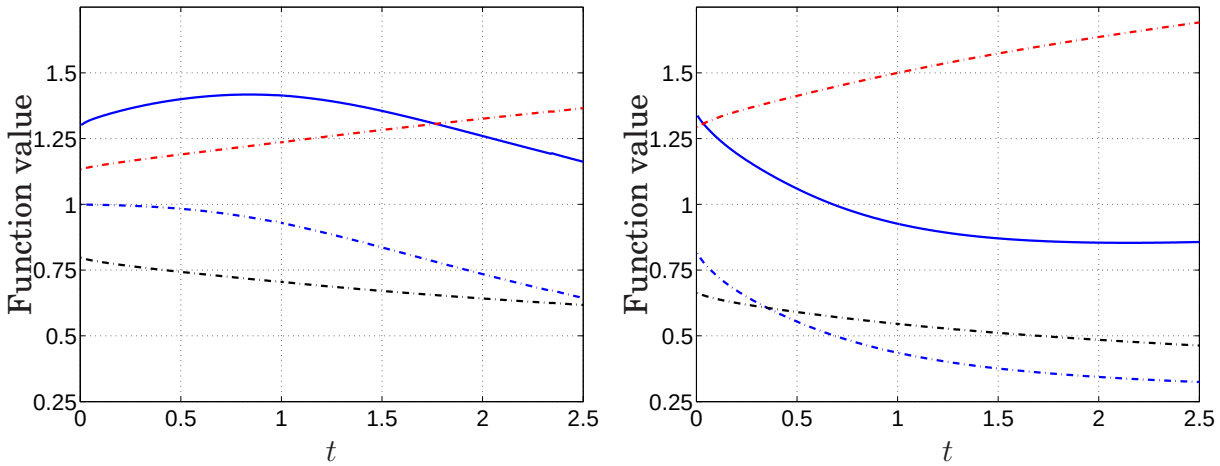

(a) 32^3 grid. (b) 64^3 grid.

Figure 5.3: Correction and damping functions from DHIT using PDH with Ψ_{PDH} active and $C_{LES} = 0.70$. — : Ψ_{PDH}; - - - : f_k; - - - : f_ω; - - - : f_μ.

5.2 Fully developed channel flow

Two Reynolds numbers have been analyzed; $Re_\tau = 950$ and $Re_\tau = 8000$, based on friction velocity u_τ and half channel height δ. The meshes used in the simulations are presented in Table 5.2. Periodic boundary conditions are applied in the stream-wise and span-wise directions. In addition, a driving pressure gradient is applied in the stream-wise direction to achieve fully developed plane channel flow. Adiabatic no-slip conditions are applied on the bottom and top walls. Due to the prescribed driving pressure gradient in the stream-wise direction, the velocity profile and the bulk velocity are not pre-defined, but rather model dependent. This is also the purpose and the motivation for the test case; to evaluate how well the proposed model captures the log-law.

For the lower Reynolds number, LES based on PDH model, i.e. the used length scale used is according to Eq. 4.10, has been applied down to the wall and four different LES length scales have been evaluated; Δ_{max}, Δ_{vol}, Δ_ω and Δ_{dw} (Eqs. 2.3, 2.13, 2.14 and 2.15). Time averaged velocity profiles and resolved stresses from the

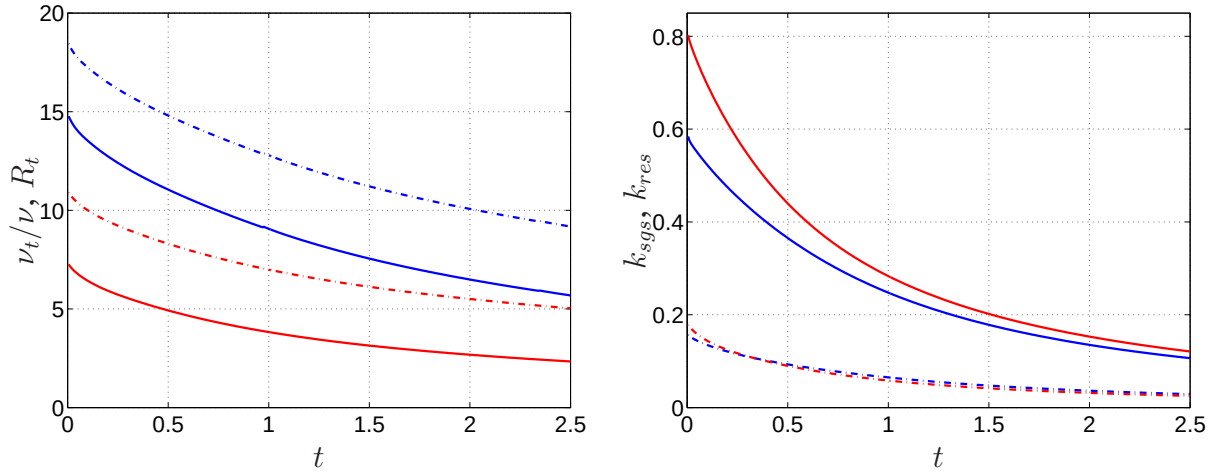

(a) —— : ν_t/ν (32^3); —— : ν_t/ν (64^3); - - - : R_t (32^3); - - - : R_t (64^3).

(b) —— : k_{res} (32^3); —— : k_{res} (64^3); - - - : k_{mod} (32^3); - - - : k_{mod} (64^3).

Figure 5.4: DHIT using PDH with Ψ_{PDH} active and $C_{LES} = 0.70$. (a) Turbulent viscosity and turbulent Reynolds number. (b) Turbulent kinetic energy.

Table 5.2: Meshes used in fully developed channel flow.

Re_τ	$(x/\delta, y/\delta, z/\delta)$	(n_x, n_y, n_z)	$(\Delta x^+, \Delta y^+, \Delta z^+)$
950	$(3.2, 2, 1.6)$	$(64, 82, 64)$	$(48, 0.60 - 103, 24)$
8000	$(3.2, 2, 1.6)$	$(64, 96, 64)$	$(400, 1.7 - 1050, 200)$

simulations are compared to DNS data by Hoyas and Jimenez [42]. The proposed subgrid-scale model is also compared to the dynamic Smagorinsky model [43] and the WALE model [44] to put the discrepancies from DNS data in a relevant perspective.

The length scale used in the LES simulations includes the correction function, Ψ_{PDH}. This function is derived assuming local equilibrium. However, close to the wall, local equilibrium is not fulfilled, see Figure 5.13. To avoid low Reynolds number damping in the off-wall region and not violating the assumption of local equilibrium, a more appropriate approach is to set the damping functions to unity. Nevertheless, the correction function is used in the LES length scale for the periodic channel flow for pure LES presented in this work. This is motivated by the channel flow in which an embedded LES approach is used. In this flow case with embedded LES, RANS and LES are combined and the correction function is applied. Furthermore, the embedded LES flow case should be able to be compared to fully developed channel flow. Moreover, the proposed model is not intended for pure LES flows but for hybrid RANS-LES modeling at high Reynolds numbers, and the embedded channel flow case in this work is only used to evaluate the suitability of the correction function over the RANS-LES interface and other interface parameters. A comparison of fully developed channel flow at $Re_\tau = 950$, where one simulation has been made with the

correction function activated and another where the damping functions are set to unity, is presented in the next section.

The near-wall behaviour is important for accurately capturing the velocity profile. The use of low Reynolds number damping functions therefore play an important role and are partly responsible for accurate near-wall modeling. On the other hand, the low Reynolds number damping functions can have effects on off-wall flows, such as free shear flow or wake flow, where low-Re effects can occur. Due to the introduction of Ψ_{PDH}, the effect of the low Reynolds number damping are canceled in LES mode. The evaluation of different LES length scales in pure LES flow is therefore made to find LES length scales that can reproduce a correct near-wall behaviour.

For Reynolds number $Re_\tau = 8000$, which aims at hybrid RANS-LES modeling, the standard DES switch (Eq. 2.2) and a zonal formulation with three prescribed switch locations were applied. The zonal formulation was used in order to evaluate the influence of switch location on the model behaviour. On the mesh used, the standard DES switch gave a transition from RANS to LES at $y^+ = 180$ and $y^+ = 250$ using PDH-LRN and MSST as base RANS models, respectively. The three prescribed locations were chosen so that transition occurred at $y^+ = 250$, $y^+ = 520$ and $y^+ = 1050$. At these three locations, the Δ_{max} and Δ_{dw} length scales were evaluated. Moreover, the length scales based on the cubic root of the cell volume and the direction of the vorticity vector were evaluated for the switch location at $y^+ = 520$. The purpose of the LES length scale evaluation is to minimize the log-layer mismatch. In order to quantify the intensity of the log-layer mismatch, the measure of skin friction reduction was used, as in Nikitin et al. [34]. Instead of extrapolating DNS data, the log-law was used to compute the center line velocity and the skin friction coefficient.

$$U^+_{cl,th} = \frac{\log\left(Re_\tau\right)}{\kappa} + 5.2 \quad \Longrightarrow \quad C_{f,th} = \frac{2}{\left(U^+_{cl,th}\right)^2} \tag{5.1}$$

$Re_\tau = 8000$ and $\kappa = 0.41$. The skin friction reduction was computed as; $\Delta C_f = (C_f - C_{f,th})/C_{f,th}$, where $C_{f,th}$ refers to the theoretical skin friction calculated from $U^+_{cl,th}$ and C_f is the skin-friction coefficient computed from the simulations presented.

Due to the wide use of Menter's $k-\omega$ SST model as a base RANS model in aerodynamic hybrid RANS-LES applications, it was used for comparison with the model proposed in this study. However, the aim of this comparison is not to evaluate whether PDH-LRN or MSST is best suited as a base RANS model for hybrid RANS-LES modeling. Instead, MSST is used to show that the hybrid RANS-LES formulation based on PDH-LRN has correct RANS-LES switch characteristics and that the proposed subgrid-scale model works as expected.

5.2.1 $Re_\tau = 950$

To clarify the effect of the correction function when LES is used down to the wall, this section starts to compare results where all damping functions are set to unity and where the correction function has been used. In the velocity profiles, shown in Figure 5.5 (a), differences are observed in the buffer region and in the lower log-layer

region. Further away from the wall, the slope in the log-layer region and the center line velocities are similar in the two simulations. A larger difference is observed in the turbulent viscosity shown in Figure 5.5 (b). An overall higher level of turbulent viscosity is predicted with the damping functions set to unity. The effect of the higher turbulent viscosity is reflected in the modeled and resolved stresses presented in Figure 5.6. A slightly higher level of resolved shear stress is recognized when the correction function is activated. Looking at the RMS values of the normal stresses, these are also higher and better predicted with the correction function activated. The peak of the stream-wise fluctuations is somewhat higher when the correction function is used compared to when the damping functions are set to unity. It is also observed that the peak is shifted to slightly lower y^+-values when Ψ_{PDH} is activated. Overall, the differences are small between the two simulations, especially for the velocity profiles.

Taking into account that the purpose of the pure LES in this thesis is for embedded channel flow, where no recirculation of the flow between inlet and outlet takes place and turbulent fluctuations are imposed, the differences between the use of Ψ_{PDH} and setting the damping functions to unity are then even smaller (no comparison is presented). Thus, the use of the correction function is acceptable.

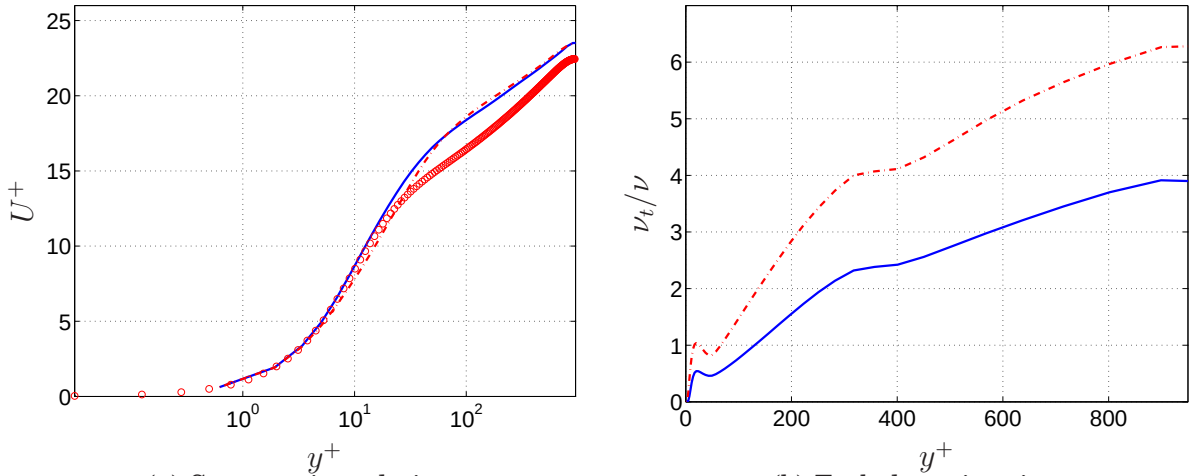

(a) Stream-wise velocity.

(b) Turbulent viscosity.

Figure 5.5: Fully developed channel flow, $Re_\tau = 950$. PDH using Δ_{dw}. —— : Ψ_{PDH} activated; - - - : $f_k = f_\omega = f_\mu$. (a) Stream-wise time averaged velocity. (b) Turbulent viscosity. Markers are DNS data [42].

The influence of using different LES length scales is strong. The best predicted velocity profile is given with $\Delta = \Delta_{dw}$ as shown in Figure 5.7 (a). The largest difference for Δ_{dw} is observed at $y^+ = 75$, where the velocity is overpredicted by 12 percent. At the channel mid section, the overprediction is reduced to 4.5 percent. Using the local maximum cell size, the maximum velocity is in good agreement with DNS data, but the buffer region and the lower log-layer region are far from well predicted. The prediction of the viscous sublayer and the buffer layer using Δ_{vol} and Δ_ω, is similar to that predicted by $\Delta = \Delta_{dw}$. However, the overpredicted velocity in the

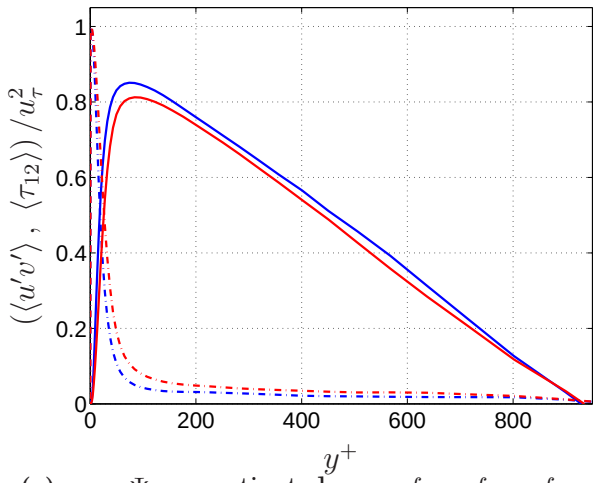

(a) —— : Ψ_{PDH} activated; —— : $f_k = f_\omega = f_\mu = 1$.

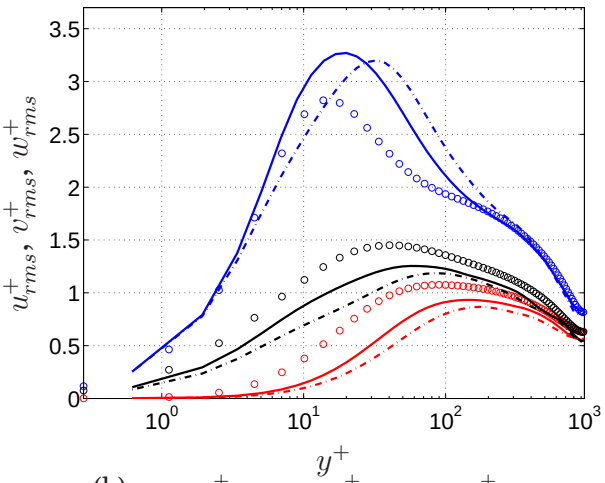

(b) —— : u^+_{rms}; —— : v^+_{rms}; —— : w^+_{rms}.

Figure 5.6: Fully developed channel flow, $Re_\tau = 950$. (a) Resolved (solid lines) and modeled+viscous (dash-dotted lines) shear stress. (b) RMS of resolved turbulent fluctuations. Solid lines: Ψ_{PDH} activated; dash-dotted lines: $f_k = f_\omega = f_\mu = 1$. Markers are DNS data [42].

log-layer region is greater using the volume and vorticity based formulations. Figure 5.7 (b) presents a comparison of PDH using Δ_{dw} and the dynamic Smagorinsky model and the WALE model. Is is observed that the proposed model has improved the prediction of the velocity profile, especially at the channel center line.

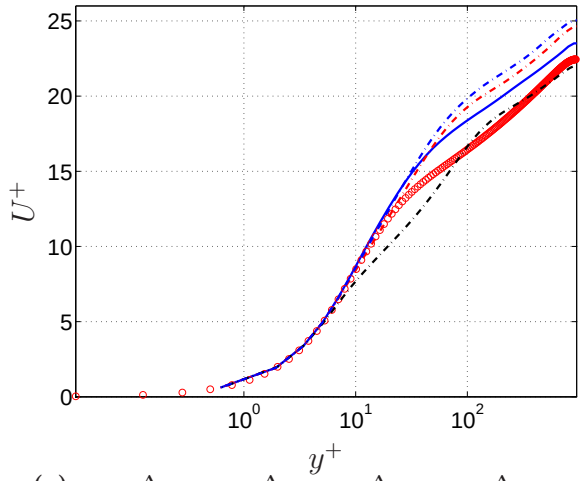

(a) —— : Δ_{dw}; - - - : Δ_ω; - - - : Δ_{vol}; - - - : Δ_{max}.

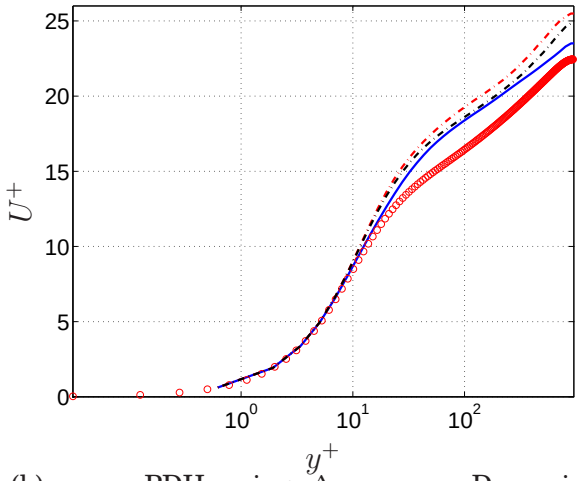

(b) —— : PDH using Δ_{dw}; - - - : Dynamic Smagorinsky; - - - : WALE.

Figure 5.7: Fully developed channel flow, $Re_\tau = 950$. Stream-wise time averaged velocity. (a) PDH using different length scales. (b) Comparison of different subgrid-scale models. Markers are DNS data [42].

The improved prediction achieved with Δ_{dw} is due to the choice of length scale in

the near-wall region. The length scale does not increase as abruptly as the volume and vorticity based formulations do since it only depends on the wall-parallel cell size for the first cells away from the wall ($C_w\Delta_{max}$). As seen in Figure 5.8, the turbulent viscosity predicted with Δ_{vol} and Δ_ω rises to $\nu_t/\nu = 2$ at already $y^+ = 35$ while, for the Δ_{dw} formulation, this level of turbulent viscosity is reach at $y^+ = 250$. These high levels of turbulent viscosity affect the resolving capability of the model. It is clear that the resolved turbulent fluctuations are higher, especially v^+_{rms} and w^+_{rms}, for Δ_{dw} than the other three length scales, as presented in Figure 5.9. This is also observed in the higher amount of resolved shear stress shown in Figure 5.10, and the resolved turbulent kinetic energy shown in Figure 5.11. The much lower turbulent viscosity seen in Figure 5.8 thus reflects the level of subgrid-scale turbulent kinetic energy, shown in Figure 5.12 (a). The length scale based on Δ_{dw} predicts the peak of subgrid-scale turbulent kinetic energy 40 percent lower compared to Δ_{vol} and Δ_ω, and 65 percent lower than the length scale based on the local maximum cell size. The only length scale that manages to preserve the DNS shape of the profiles of the resolved turbulent fluctuations through the whole channel is Δ_{dw}, as presented in Figure 5.9. The v and w components, are somewhat under resolved with Δ_{dw}, but in line with the dynamic Smagorinsky model and the WALE model. For $y^+ > 200$, almost perfect agreement is seen for u^+_{rms} with the proposed model. The peak level is somewhat overpredicted but in better agreement with DNS data than both the dynamic Smagorinsky model and the WALE model. Moreover, a slight shift of the peak towards higher y^+-values is observed. This is a trend also recognized for the dynamic Smagorinsky and WALE models.

It is observed that the PDH damping functions not reach unity in the off-wall region due to the low turbulent Reynolds numbers, see Figure 5.12 (b). By accident, the correction function takes values close to one, which corresponds to the region just to the left of the minimum value of Ψ_{PDH} (Figure 4.1). In the very close vicinity of the wall, $R_t \to 0$ and $\Psi_{PDH} \to 10$, which is in agreement with the numerical limiter used in Eq. 4.19.

Budgets of subgrid-scale properties in the k and ω equations for the proposed model are plotted in Figure 5.13. For comparison, budgets from DNS data [42], corresponding to the terms in the k-equation of the proposed model, are shown in Figure 5.14. The assumption about local equilibrium holds for both the k and ω equations for $y^+ \geq 20$. Moreover, local equilibrium occurs approximately simultaneously in both equations. Thus, the assumption used to derive the correction function, Ψ_{PDH}, is satisfied.

Analyzing the equation for turbulent kinetic energy, viscous and turbulent diffusion come into play when $y^+ \leq 20$. This is somewhat closer to the wall compared to DNS data. The peak of the production term in the k-equation for the proposed model occurs at almost the same location from the wall as in DNS data, i.e. at approximately $y^+ = 10$. Overall, the levels of the k-equation terms in the proposed model are lower than in DNS since only the modeled parts are presented. Budgets for the ω-equation show that the viscous diffusion and the destruction terms dominate in the vicinity of the wall. The dissipation rate takes a large value on the wall but is

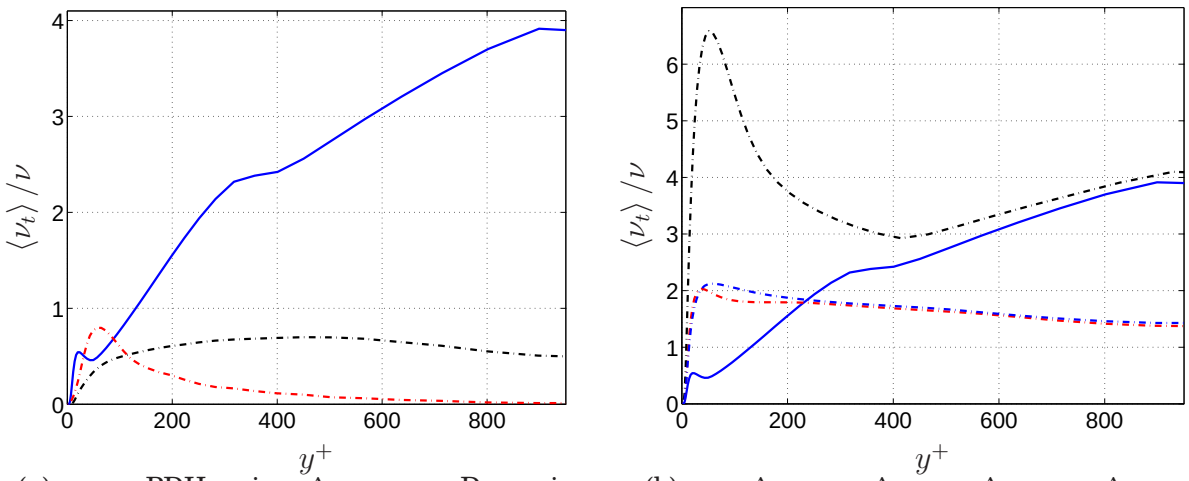

(a) —— : PDH using Δ_{dw}; - - - : Dynamic Smagorinsky; - - - : WALE.

(b) —— : Δ_{dw}; - - - : Δ_{ω}; - - - : Δ_{vol}; - - - : Δ_{max}.

Figure 5.8: Fully developed channel flow, $Re_\tau = 950$. Turbulent viscosity. (a) Comparison of different subgrid-scale models. (b) PDH using different length scales.

close to zero at already $y^+ = 20$. Since the viscous diffusion depends on the second derivative of ω, this term has to be large in the near-wall region. The destruction of ω is proportional to ω^2, hence it also has to be large close to the wall. Compared to the other terms in the ω-equation, the turbulent diffusion and the cross-diffusion terms play a less important role in the vicinity of the wall.

5.2.2 $Re_\tau = 8000$

To demonstrate the characteristics of PDH based hybrid RANS-LES, the evaluation for $Re_\tau = 8000$ starts with a comparison of a zonal formulation based on PDH and MSST as base models. For these simulations, the RANS-LES switch is prescribed to occur at $y^+ = 520$, and Δ_{max} has been used as the LES length scale.

The PDH based zonal formulation performs similar to the formulation based on MSST. In Figure 5.15, a slight difference is observed at the RANS-LES interface. The kink related to the MSST based formulation is shifted towards lower y^+-values compared to PDH. PDH, on the other hand, gives a steeper gradient of the velocity at the interface. Similar center line velocities are achieved with both models, and the skin friction reduction, due to the log-layer mismatch, is hence also comparable with a somewhat lower value for the PDH based formulation (see Table 5.3).

MSST gives a lower turbulent viscosity in the RANS region, and the turbulent viscosity reduction at the interface is steeper, as shown in Figure 5.16 (a). The lower turbulent viscosity and the steeper gradient at the interface is reflected in Figure 5.16 (b), where resolved and modeled shear stress are presented. The higher turbulent viscosity level given by the PDH model gives a lower peak of resolved shear stress compared to MSST. The ratio of resolved to modeled shear stress at the interface is also lower for the PDH formulation since the level of the turbulent viscosity

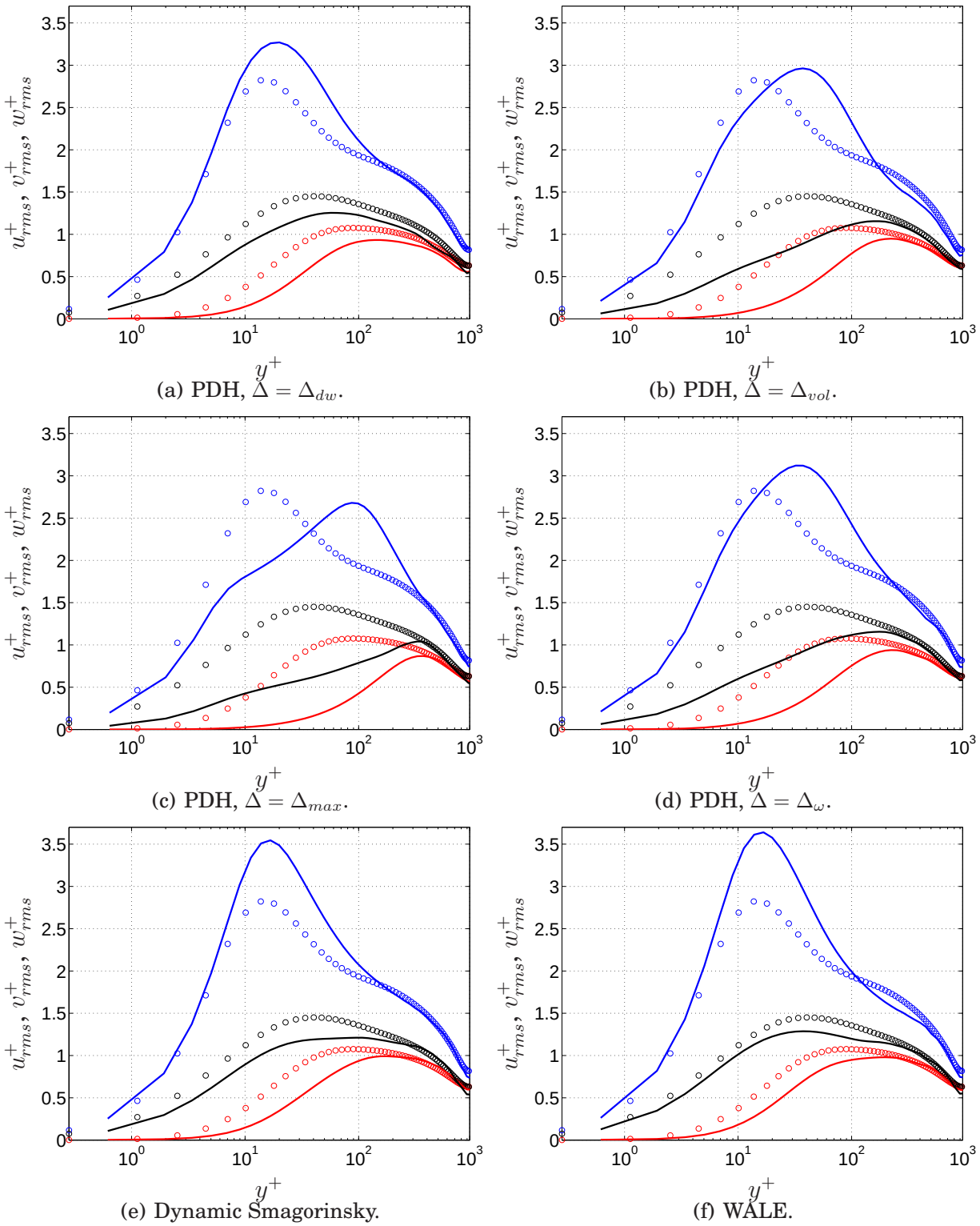

(a) PDH, $\tilde{\Delta} = \Delta_{dw}$.

(b) PDH, $\tilde{\Delta} = \Delta_{vol}$.

(c) PDH, $\tilde{\Delta} = \Delta_{max}$.

(d) PDH, $\tilde{\Delta} = \Delta_{\omega}$.

(e) Dynamic Smagorinsky.

(f) WALE.

Figure 5.9: Fully developed channel flow, $Re_\tau = 950$. Resolved turbulent fluctuations. — : u^+_{rms}; — : v^+_{rms}; — : w^+_{rms}. Markers are DNS data [42].

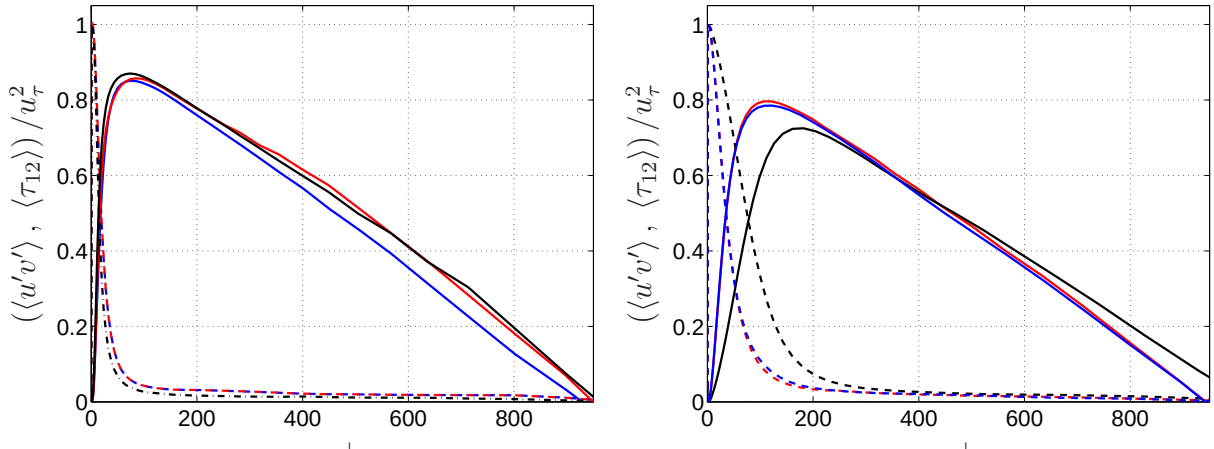

(a) ——: PDH using Δ_{dw}; ——: Dynamic Smagorinsky; ——: WALE.

(b) ——: Δ_ω; ——: Δ_{vol}; ——: Δ_{max}.

Figure 5.10: Fully developed channel flow, $Re_\tau = 950$. Resolved (solid lines) and modeled+viscous (dash-dotted lines) shear stress. (a) Comparison of different subgrid-scale models. (b) PDH using different length scales.

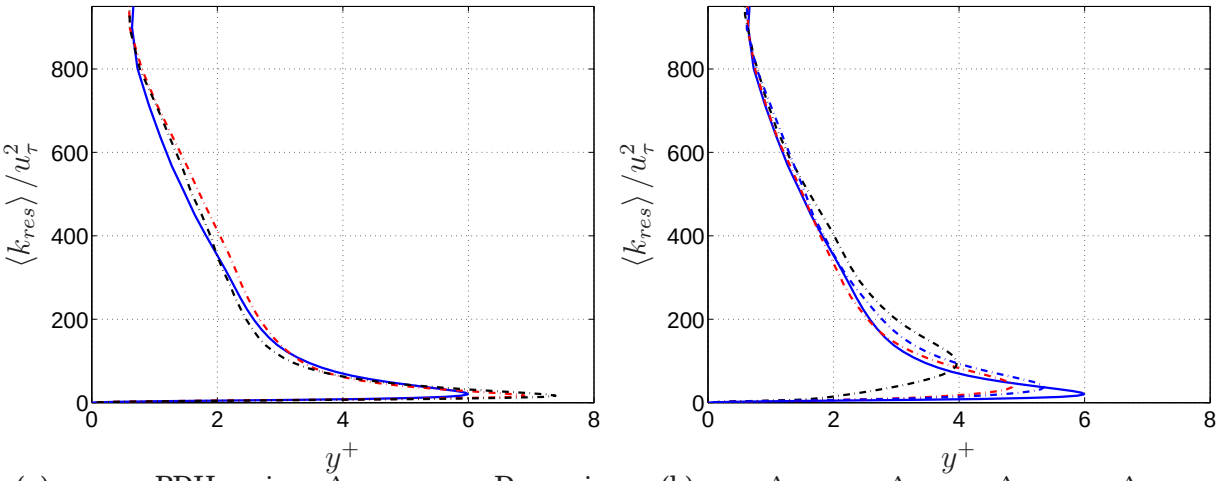

(a) ——: PDH using Δ_{dw}; - - -: Dynamic Smagorinsky; - - -: WALE.

(b) ——: Δ_{dw}; - - -: Δ_ω; - - -: Δ_{vol}; - - -: Δ_{max}.

Figure 5.11: Fully developed channel flow, $Re_\tau = 950$. Resolved turbulent kinetic energy. (a) Comparison of different subgrid-scale models. (b) PDH using different length scales.

is higher at the RANS-LES interface.

The overall behaviour of the hybrid RANS-LES formulation based on PDH is comparable with MSST. Both subgrid-scale models performance well and most of the differences observed in the results can be related to the RANS zone where clear differences are present between the models.

From this brief analysis, made to justify a reasonable behaviour of PDH as base model, a more thorough analysis of the simulations performed with the proposed

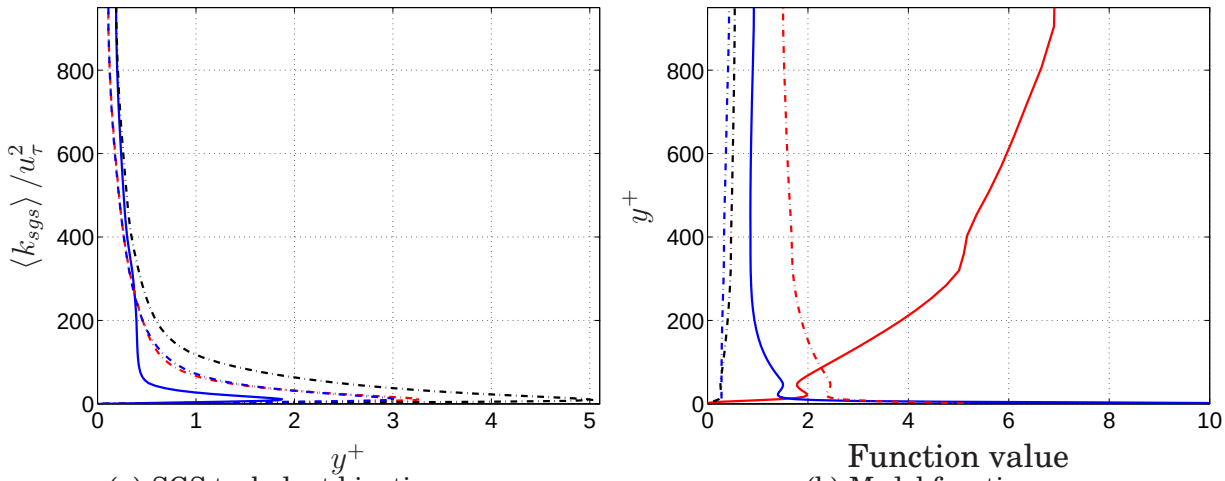

(a) SGS turbulent kinetic energy.

(b) Model functions.

Figure 5.12: Fully developed channel flow, $Re_\tau = 950$ using PDH. (a) Subgrid-scale turbulent kinetic energy using different length scales. —— : Δ_{dw}; - · - : Δ_ω; - - - : Δ_{vol}; - · · - : Δ_{max}. (b) Correction function, turbulent Reynolds number and damping functions. —— : Ψ_{PDH}; —— : Re_t; - · - : f_k; - - - : f_ω; - · · - : f_μ.

model will now be presented.

The abrupt increase in velocity in the log-law region seen in Figure 5.17 indicates a log-layer mismatch. Figure 5.17 (a), shows different locations at which the model switch from RANS to LES using Δ_{max}. Comparing the computed skin friction reduction for Δ_{max} presented in Table 5.3, it is observed that the log-layer mismatch is increased when the switch is moved closer to the wall. Analyzing Figure 5.17 (b), where different interface locations are compared for Δ_{dw}, it is seen that the best predicted velocity profile is given for the RANS-LES switch at $y^+ = 250$, while for the switch locations at $y^+ = 520$ and 1050, the overpredictions are enhanced. With the RANS-LES interface at $y^+ = 1050$, a reasonable agreement with the log-law is achieved with Δ_{max}. A larger overprediction of the center line velocity is given with Δ_{dw} at this location, which results in an increased reduction of the skin friction coefficient, see Table 5.3. Weaker kinks are observed at the interface for Δ_{dw} compared to Δ_{max}. However, the profile given by Δ_{dw} for the interface at $y^+ = 1050$ gets a second kink, which results in a slightly higher center line velocity compared to Δ_{max}.

Figure 5.17 (c) presents velocity profiles for Δ_{vol} and Δ_ω with the RANS-LES switch located at $y^+ = 520$. The formulations behave very similarly and over estimates the maximum velocity as the formulation based on the local maximum cell size. The kink at the interface is somewhat milder compared to Δ_{max}, but the total skin friction reduction is larger, as seen in Table 5.3. The worst log-layer mismatch is seen with the DES switch (Eq. 2.2), see Figure 5.17 (d). Using PDH and MSST as base models, the switch from RANS to LES is made at $y^+ = 180$ and 250, respectively. The shapes of both velocity profiles are similar, as is the maximum velocity. The stronger log-layer mismatch and the increased overprediction of the velocity profile, using the DES compared to the zonal formulations, are due to the switch

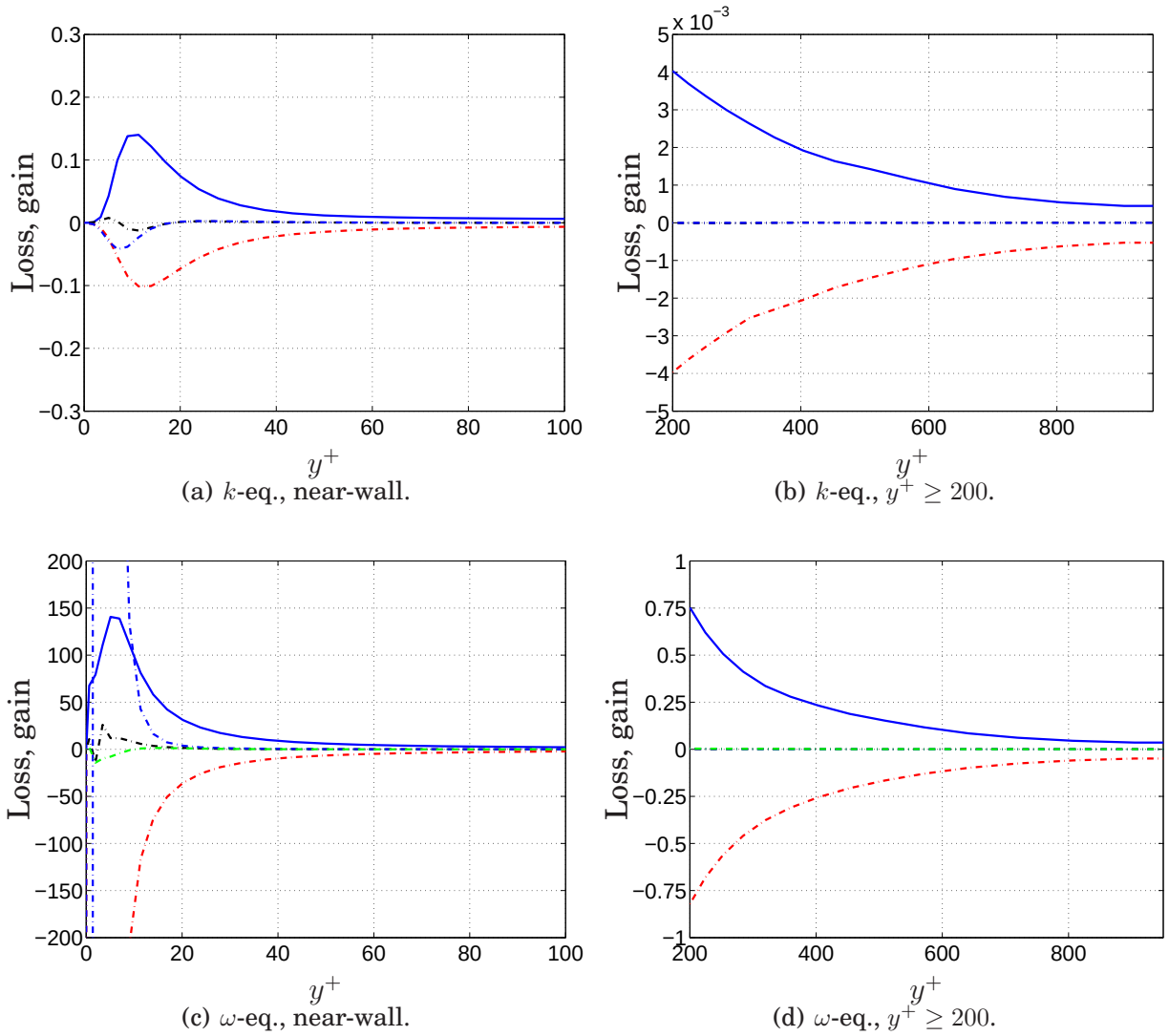

(a) k-eq., near-wall. (b) k-eq., $y^+ \geq 200$.

(c) ω-eq., near-wall. (d) ω-eq., $y^+ \geq 200$.

Figure 5.13: Fully developed channel flow, $Re_\tau = 950$. Budgets of subgrid-scale properties for PDH using Δ_{dw}. —— : production; - - - : dissipation/destruction; - - - : turbulent diffusion; - - - : viscous diffusion. - - - : cross diffusion. (a) and (b) k-equation, (c) and (d) ω-equation.

location, which is made closer to the wall, and the use of Δ_{max}.

The local maximum cell size gives a slow reduction of the turbulent viscosity at the interface (Figure 5.18 (d)) and therefore a low ratio of resolved to modeled turbulent stresses, as seen in Figure 5.19 (d). Even though the velocity profiles are substantially overpredicted in the LES region using DES, the results are in agreement with Nikitin et al. [34] in their study of DES as a WMLES approach.

The level of turbulent viscosity produced is essentially the core of the log-layer mismatch issue. Analyzing Figure 5.18, large differences are observed between the LES length-scale formulations. For the RANS-LES switch at $y^+ = 520$ and 1050, it is observed that the different LES length scale formulations have only a small effect on

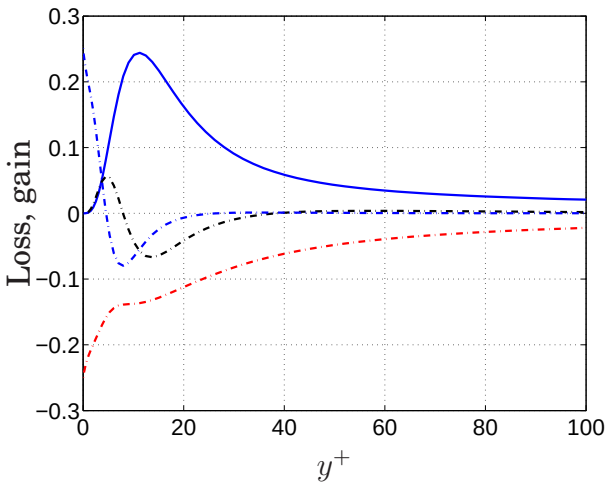

Figure 5.14: Budget of DNS data corresponding to k-equation terms in fully developed channel flow at $Re_\tau = 950$. —: production; - - -: dissipation; - - -: turbulent diffusion; - - -: viscous diffusion.

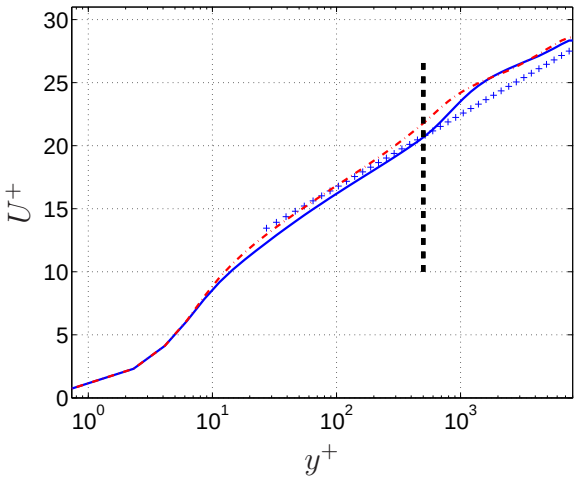

Figure 5.15: Fully developed channel flow, $Re_\tau = 8000$. Comparison of PDH and MSST based zonal hybrid RANS-LES. Interface at $y^+ = 520$, $\Delta = \Delta_{max}$. Stream-wise time averaged velocity. —: PDH; - - -: MSST. Interface location indicated by dashed black line.

the maximum turbulent viscosity produced in the RANS zone. The range of RANS peak levels for $y^+ = 520$ are $72 \leq \nu_t/\nu \leq 90$. The large differences are recognized in the interface and bulk flow regions. For $y^+ = 520$ with Δ_{dw}, the turbulent viscosity goes down from $\nu_t/\nu = 72$ in the RANS zone to only $\nu_t/\nu = 10$ in the LES zone at $y^+ = 900$. Comparing Δ_{vol} and Δ_ω, almost the same RANS levels of turbulent viscosity are given with slightly lower values in the LES region for Δ_{vol}. Their reduction of ν_t/ν at the interface are almost as fast as for Δ_{dw}, but the lowest level reached in the interface region at $y^+ = 900$ is about $\nu_t/\nu = 20$ instead of 10 as for Δ_{dw}. With Δ_{max}, the slowest reduction of turbulent viscosity is observed at the interface. The

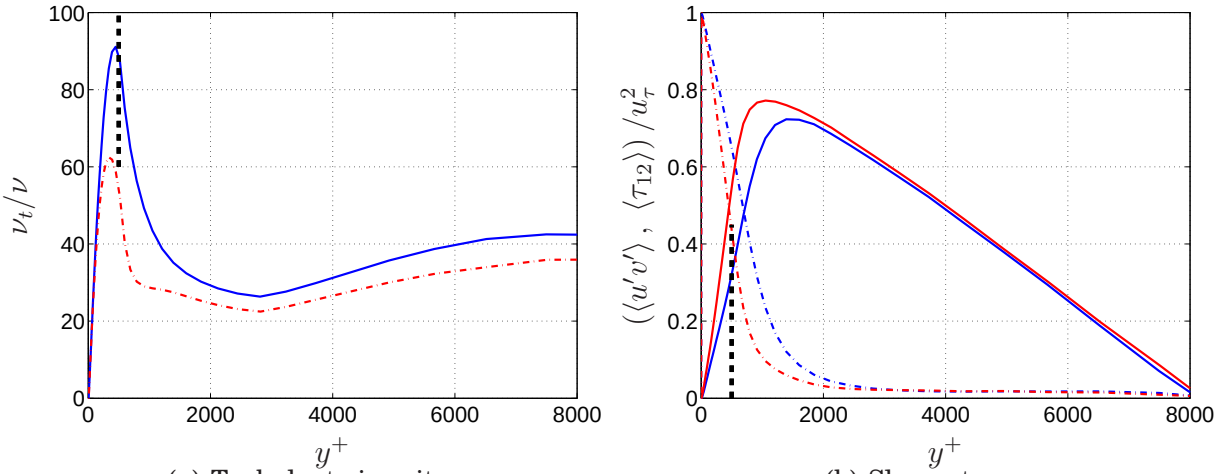

(a) Turbulent viscosity.

(b) Shear stress.

Figure 5.16: Fully developed channel flow, $Re_\tau = 8000$. Comparison of PDH and MSST based zonal hybrid RANS-LES. Interface at $y^+ = 520$, $\Delta = \Delta_{max}$. —— : PDH; - - - : MSST. (a) Turbulent viscosity. (b) Resolved (solid lines) and modeled+viscous (dash-dotted lines) shear stress. Interface location indicated by dashed black line.

Table 5.3: Summary of simulations at $Re_\tau = 8000$

RANS model	Formulation	Δ_{LES}	y^+_{switch}	ΔC_f^*
PDH	Zonal	Δ_{max}	250	-13.7%
PDH	Zonal	Δ_{max}	520	-8.4%
PDH	Zonal	Δ_{max}	1050	-5.4%
PDH	Zonal	Δ_{dw}	250	-1.8%
PDH	Zonal	Δ_{dw}	520	-4.0%
PDH	Zonal	Δ_{dw}	1050	-7.4%
PDH	Zonal	Δ_{vol}	520	-8.6%
PDH	Zonal	Δ_{ω}	520	-10.3%
MSST	Zonal	Δ_{max}	520	-9.9%
PDH	DES	Δ_{max}	180	-14.9%
MSST	DES	Δ_{max}	250	-14.9%

*see Eq. 5.1.

highest levels of turbulent viscosity are also given in the RANS and LES regions. However, the levels reached at the center line are similar with Δ_{max} and Δ_{dw} since the maximum local cell size is applied here with both length scale formulations (see Eq. 2.3 and 2.15).

Figure 5.19 shows modeled and resolved shear stress. The rapid reduction in ν_t with Δ_{dw} is clearly reflected in the shear-stress levels seen in Figure 5.19 (b). The LES length scale based on Δ_{dw} gives the highest peak of resolved shear stress of all four length scales. With the interface at $y^+ = 520$, the resolved shear stress al-

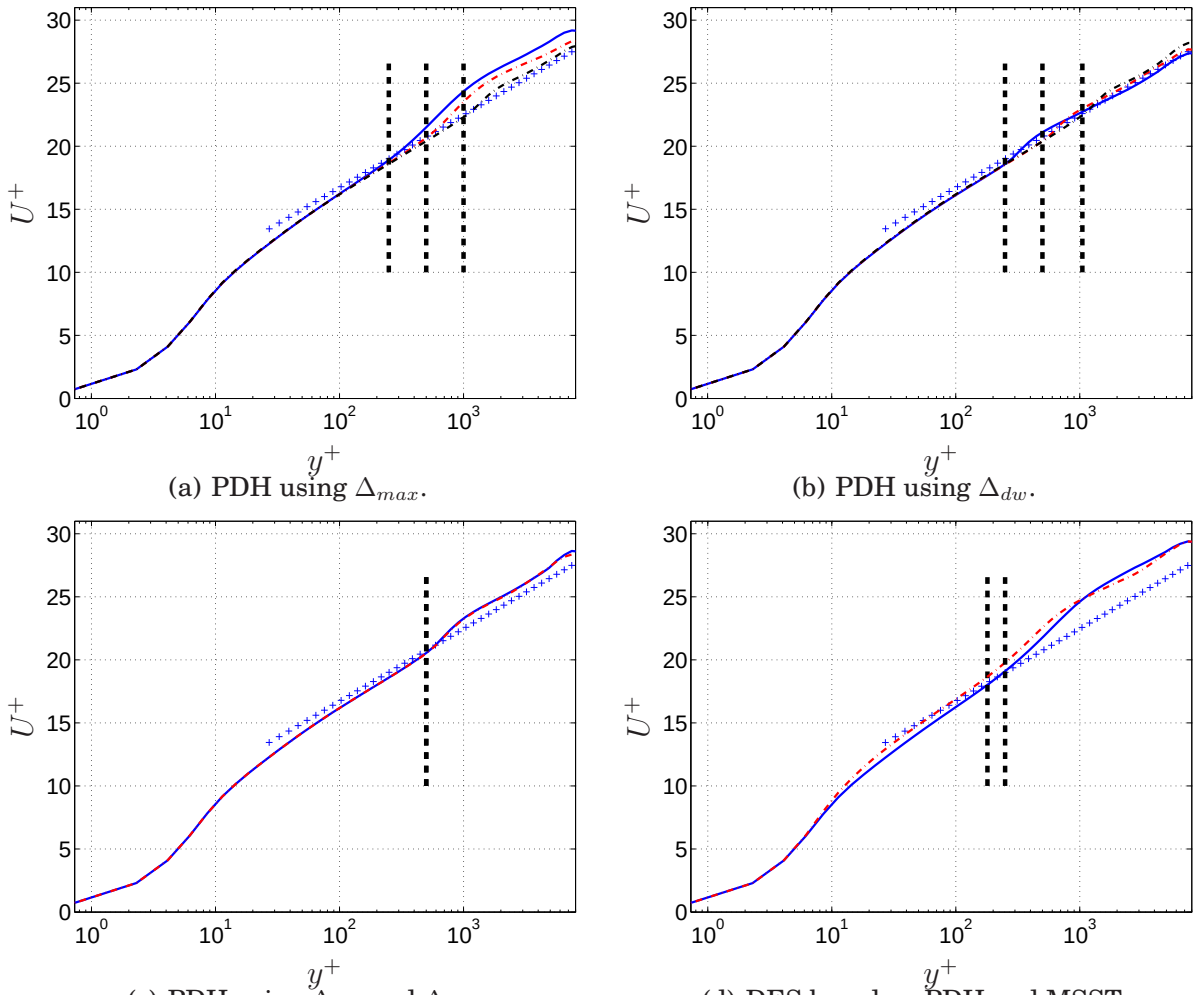

(a) PDH using Δ_{max}.

(b) PDH using Δ_{dw}.

(c) PDH using Δ_{vol} and Δ_{ω}.

(d) DES based on PDH and MSST.

Figure 5.17: Fully developed channel flow, $Re_\tau = 8000$. Stream-wise time-averaged velocity. (a) PDH using Δ_{max} with different switch locations. —: $y^+ = 250$; - - -: $y^+ = 520$; - - -: $y^+ = 1050$. (b) PDH using Δ_{dw} with different switch locations. —: $y^+ = 250$; - - -: $y^+ = 520$; - - -: $y^+ = 1050$. (c) Switch location at $y^+ = 520$ using PDH. —: Δ_{ω}; - - -: Δ_{vol}. (d) DES using PDH and MSST as base models. —: PDH; - - -: MSST. Switch location indicated by dashed black line.

ready represents 55 percent of the total shear stress level with Δ_{dw}, which should be compared to 33 percent for Δ_{max}. A slightly higher level of resolved shear stress is observed for Δ_{vol} than for Δ_{ω}, which is also reflected in the velocity profiles, where the latter suffers from a stronger log-layer mismatch. Even though the off-wall turbulent viscosity with Δ_{vol} and Δ_{ω} is only 32 percent of that produced with Δ_{dw}, Figure 5.19 shows a negligible difference in the modeled stress levels between different filter widths. This is caused by the modeled stresses' dependency on the velocity gradients. Those are weak in the LES region where the maximum turbulent viscosity is present, and thus small discrepancies are observed in this region compared to the interface region. Moreover, it can be concluded that the lower level of ν_t produced

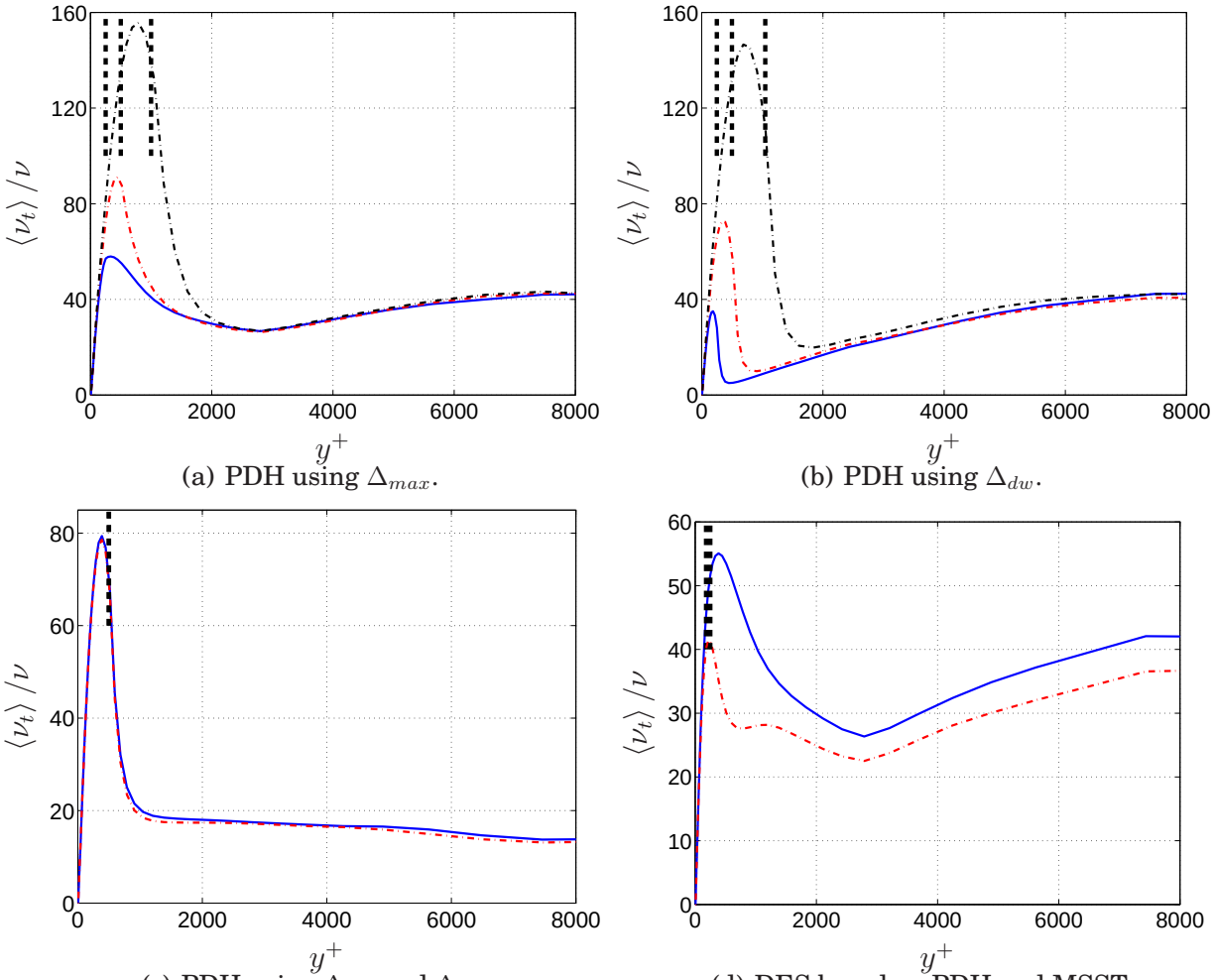

(a) PDH using Δ_{max}.

(b) PDH using Δ_{dw}.

(c) PDH using Δ_{vol} and Δ_{ω}.

(d) DES based on PDH and MSST.

Figure 5.18: Fully developed channel flow, $Re_\tau = 8000$. Turbulent viscosity. (a) PDH using Δ_{max} with different switch locations. —: $y^+ = 250$; - - -: $y^+ = 520$; - - -: $y^+ = 1050$. (b) PDH using Δ_{dw} with different switch locations. —: $y^+ = 250$; - - -: $y^+ = 520$; - - -: $y^+ = 1050$. (c) Switch location at $y^+ = 520$ using PDH. —: Δ_{ω}; - - -: Δ_{vol}. (d) DES using PDH and MSST as base models. —: PDH; - - -: MSST. Switch location indicated by dashed black line.

in the interface region with Δ_{dw}, compared to the other analyzed LES length scales, is the key issue in terms of generating an accurate turbulence resolving flow and to reduce the log-layer mismatch.

5.2.3 Summary

For both formulations, pure LES and zonal RANS-LES, the LES length scale based on Δ_{dw} shows a superiority to Δ_{max}, Δ_{vol} and Δ_{ω} for the analyzed grids and Reynolds numbers. The wall distance based LES length scale improves the results substantially for pure LES at $Re_\tau = 950$. The overprediction of the stream-wise velocity is

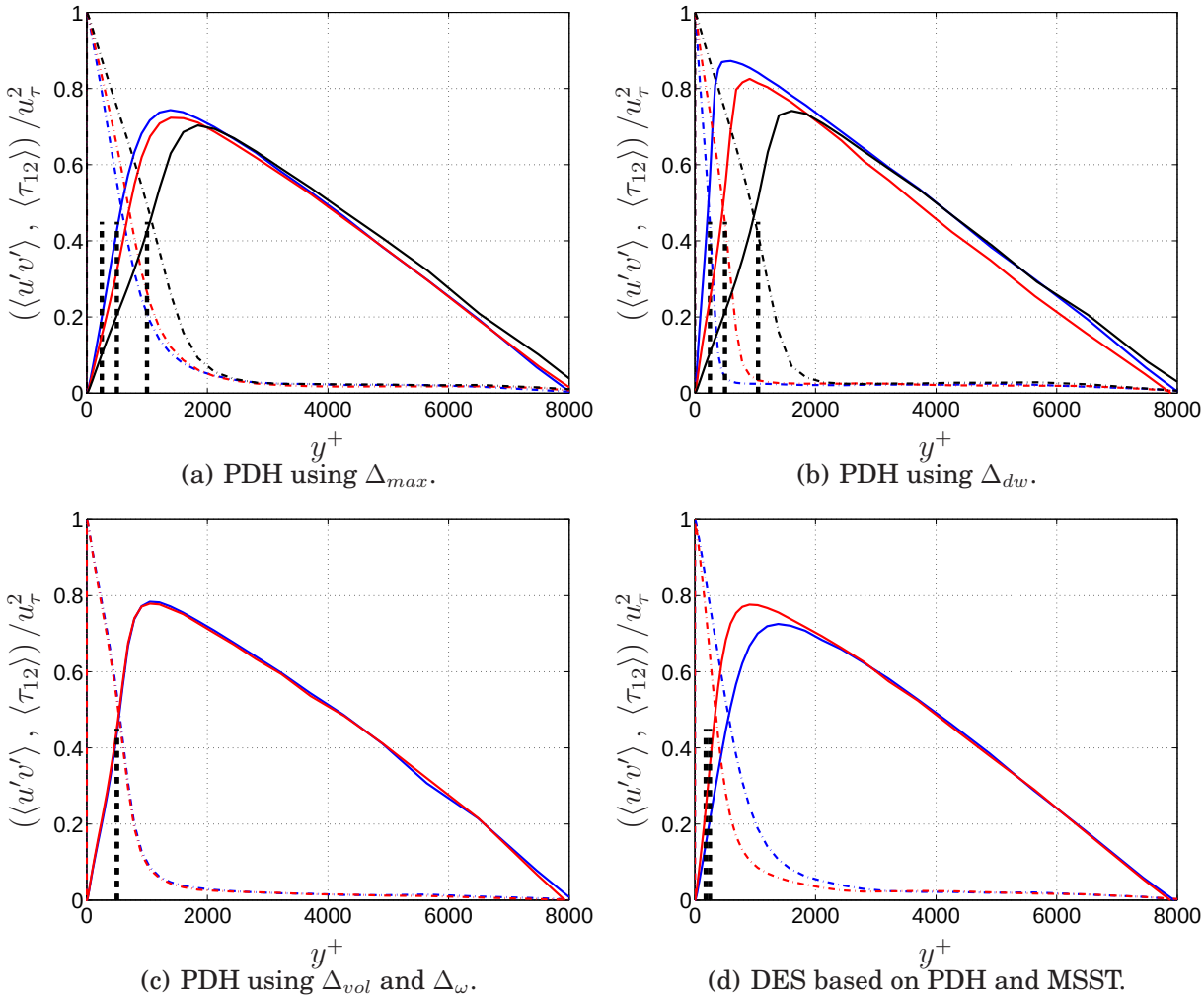

(a) PDH using Δ_{max}.

(b) PDH using Δ_{dw}.

(c) PDH using Δ_{vol} and Δ_{ω}.

(d) DES based on PDH and MSST.

Figure 5.19: Fully developed channel flow, $Re_\tau = 8000$. Resolved (solid lines) and modeled+viscous (dash-dotted lines) shear stress. (a) PDH using Δ_{max} with different switch locations. —: $y^+ = 250$; —: $y^+ = 520$; —: $y^+ = 1050$. (b) PDH using Δ_{dw} with different switch locations. —: $y^+ = 250$; —: $y^+ = 520$; —: $y^+ = 1050$. (c) Switch location at $y^+ = 520$ using PDH. —: Δ_{ω}; —: Δ_{vol}. (d) DES using PDH and MSST as base models. —: PDH; —: MSST. Switch location indicated by dashed black line.

reduced due to a well suited turbulent viscosity distribution which gives an improvement of the normal and shear stress distributions. For $Re_\tau = 8000$, it was observed that the length scale, to a large extent, influences the intensity of the log-layer mismatch. The wall distance based filter width is well suited for this application as well and reduces the log-layer mismatch compared to the other LES length scales tested.

5.3 Channel flow using embedded LES

In channel flow at low Reynolds numbers, the flow characteristics are well defined and high quality DNS data are available. As a first step towards more advanced flow cases, relying on an embedded approach, channel flow using embedded LES is explored with the proposed hybrid RANS-LES model. The channel flow of embedded LES presented in this work should be seen as a first step towards more advanced embedded LES simulations at high Reynolds numbers. The purpose of the test case is to evaluate the use of the correction function in an embedded LES approach as well as other interface parameters. For complex internal flows, an embedded approach is attractive, e.g. in the transonic duct flow case [10]. The upstream boundary layer in the referred flow case can be accurately modeled with RANS, and the separated flow in the shock region can be treated with turbulence-resolving methods.

Two equally resolved meshes were used, see Table 5.4. As the inlet boundary condition to the RANS region, a velocity profile from a precursor RANS simulation of fully developed channel flow at $Re_\tau = 950$, using PDH LRN, was applied. At $x/\delta = 1$, a RANS-LES interface plane was employed. The RANS diffusion and convection fluxes across the interface in the k and ω equations were modified to reach typical SGS levels. The subgrid-scale turbulent kinetic energy at the interface was estimated from Eq. 5.2, where $0.025 < f_{k,\,int} < 0.20$ were investigated. The interface SGS dissipation rate is computed according to Eq. 5.3. Anisotropic turbulent synthetic fluctuations [6] were added to the mean flow field at the interface as additional source terms in the continuity and momentum equations to stimulate the development of turbulence-resolving flow. The RMS values of the imposed synthetic normal stresses are constant across the channel height. The imposed synthetic shear stress ($\langle u'v' \rangle$) is constant across the channel height as well, but with a change of sign at the channel center line. In the RANS and LES regions, second order upwind (van Leer) and second order central differencing schemes were used, respectively. In the simulations, the same time step, $\Delta t = 1 \cdot 10^{-3}\ s$, was applied in both RANS and LES regions.

$$k_{sgs,int} = f_{k,int} \cdot k_{RANS} \tag{5.2}$$

$$\omega_{sgs,int} = \frac{k_{sgs,int}^{1/2}}{C_k \cdot \Psi_{PDH} C_{LES} \Delta} \tag{5.3}$$

From the LES simulations of fully developed channel flow, Δ_{dw} was concluded to be the best suited LES length scale for the proposed model. All simulations of channel flow using embedded LES presented are therefore made with $\Delta = \Delta_{dw}$. Results for $f_{k,int} = 0.050$ have been evaluated for both domains. A negligible influence of the results between the two domains was observed, and thus the evaluation of $f_{k,int}$ could be made on the smaller domain size.

In fully developed channel flow, the velocity profile is not prescribed since the flow is recirculated due to the periodic boundary conditions in the stream-wise direction. For a well converged solution of fully developed flow, the driving pressure gradient

Table 5.4: Meshes used in channel flow of embedded LES.

Re_τ	$(x/\delta, y/\delta, z/\delta)$	(n_x, n_y, n_z)	$(\Delta x^+, \Delta y^+, \Delta z^+)$	x_{int}/δ
950	$(3.2, 2, 1.6)$	$(64, 82, 64)$	$(48, 0.60 - 103, 24)$	1
950	$(6.4, 2, 1.6)$	$(128, 82, 64)$	$(48, 0.60 - 103, 24)$	1

balances the wall shear stress. In contrast, in this channel flow case of embedded LES, the velocity profile at the RANS-LES interface is prescribed from the upstream RANS domain. The driving pressure gradient, therefore, does not necessarily need to balance the wall shear stress, since the RANS and LES velocity profiles do not always coincide. This happens in the presented simulations since the LES model does not manage to re-create the RANS velocity profile, and the only way to compensate for these differences is through a change in the skin friction.

The proposed model shows a weak sensitivity to $f_{k,int}$. At $x/\Delta = 3.025$, small differences are observed in the velocity profiles and the resolved stresses, as seen in Figures 5.20 and 5.21. The turbulent viscosity produced is proportional to $f_{k,int}$. As observed in Figure 5.20 (b), an increase by a factor of two in $f_{k,int}$, almost doubles the turbulent viscosity. The low values of turbulent viscosity given in the near-wall region almost disable the subgrid-scale model, and thus the differences between different interface conditions are negligibly small in this region. Further out from the wall, the turbulent viscosity level increases and the subgrid-scale model starts to play a more important role. Analyzing Figure 5.21 (b), it is recognized that the discrepancies in resolved normal stresses between the interface conditions are distinguishable for $y > 0.1$ ($y^+ > 100$). The high RMS values observed in the off-wall region are related to the synthetic fluctuations, which have a constant RMS value across the channel height. However, the slope of u^+_{rms} is better captured with higher $f_{k,int}$. Due to the higher $f_{k,int}$, a higher level of subgrid-scale turbulent kinetic energy is prescribed at the interface, giving a higher level of turbulent viscosity, which in turn gives an increased damping effect of the velocity fluctuations. The difference in ν_t is also observed as a weak effect in the shear stress presented in Figure 5.21 (a). As for the zonal RANS-LES simulations at $Re_\tau = 8000$, the large difference in ν_t in the outer boundary layer does not have a strong influence on the modeled stresses since the velocity gradients are small in this region.

The effect of the modified fluxes of the turbulent quantities over the interfaces is plotted in Figure 5.22 (a), where the stream-wise peak level of the turbulent viscosity is presented. From the RANS level of $\nu_t/\nu = 115$, the turbulent viscosity is reduced to $\nu_t/\nu = 0.4 - 1.2$ for increased $f_{k,int}$, immediately downstream of the interface. An overshot in the turbulent viscosity is observed just upstream of the interface, reaching a value of $\nu_t/\nu = 170$ for $f_{k,int} = 0.025$. The peak is slightly increased for higher $f_{k,int}$ values. The turbulent viscosity increases downstream of the interface and the peak values reached at $x/\Delta = 3.025$ are $\nu_t/\nu = 0.7 - 4.2$ (compare the profiles presented in Figure 5.20 (b)).

The flow recovers quickly downstream of the interface, with a slight difference

between different $f_{k,int}$ values. Figure 5.22 (b), showing the stream-wise friction velocity, indicates that the LES flow only needs 1.5 boundary layer thicknesses to recover a friction velocity near unity as in the RANS region. All simulations share similar oscillations that are present for $f_{k,int} = 0.025$ in Figure 5.22. For all other cases, only every second node is plotted in the outlet region in order to make the figures clearer.

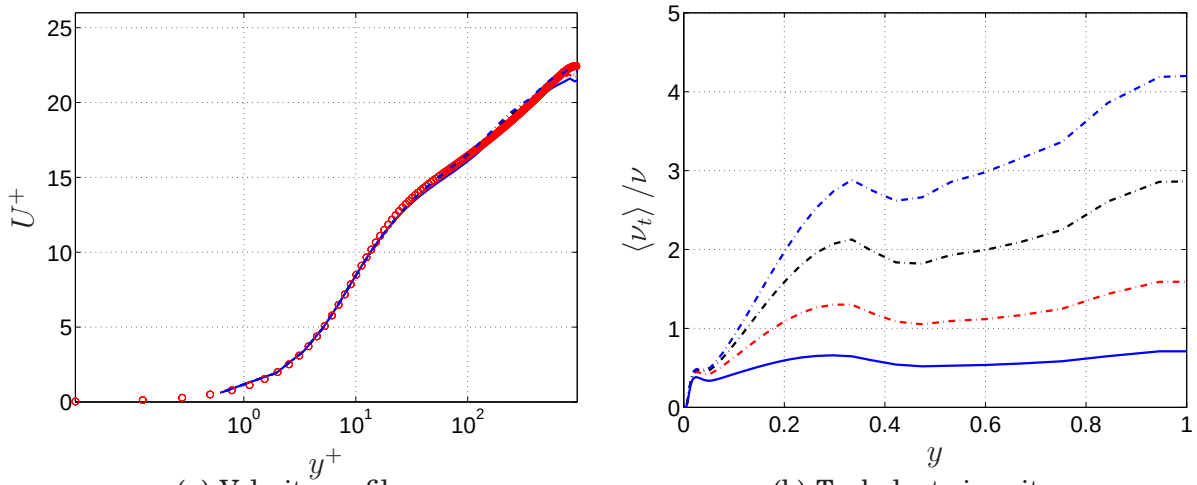

(a) Velocity profiles.

(b) Turbulent viscosity.

Figure 5.20: Channel flow using embedded LES. PDH with Δ_{dw}. Time averaged stream-wise velocity and turbulent viscosity at $x/\delta = 3.025$. —— : $f_{k,int} = 0.025$; - - - : $f_{k,int} = 0.050$; - - - : $f_{k,int} = 0.100$; - - - : $f_{k,int} = 0.200$. Markers are DNS data [42].

The RANS velocity profile shown in Figure 5.23 at $x/\delta = 0.4250$ agrees well with DNS data. No change in turbulent viscosity (Figure 5.24 (a)) and friction velocity (Figure 5.24 (b)) is observed in the RANS domain away from the interface. As expected at $x/\delta = 0.4250$, no resolved shear stress is observed, as seen in Figure 5.25 (a), since RANS is applied here. However, further downstream in the RANS region, the imposed fluctuations affect the RANS flow upstream of the interface. As reflected in Figure 5.24 (a), the maximum values of u^+_{rms} are not zero for $x/\delta < 1$.

The turbulent quantities are modified at the interface, giving an abrupt reduction of the turbulent viscosity. To compensate for the reduced modeled stresses, due to the reduction in turbulent viscosity, the resolved counter part must increase. The anisotropic synthetic turbulence is imposed to stimulate the development of the turbulence resolving flow, but cannot afford to increase the resolved stresses as much as needed to compensate for the, almost negligible, modeled part. This is an example of what in an earlier section was referred to as the grey area. However, the grey area is still small. The flow recovers in only 1.5 boundary layer thicknesses. Due to the drop in friction velocity and the too low level of resolved stresses at the interface, the velocity profile at $x/\delta = 1.275$ is overpredicted, as seen in Figure 5.23. It is also observed that the resolved shear stress shown in Figure 5.25 (a) is larger than one, which indicates a shift from the fully developed channel flow state.

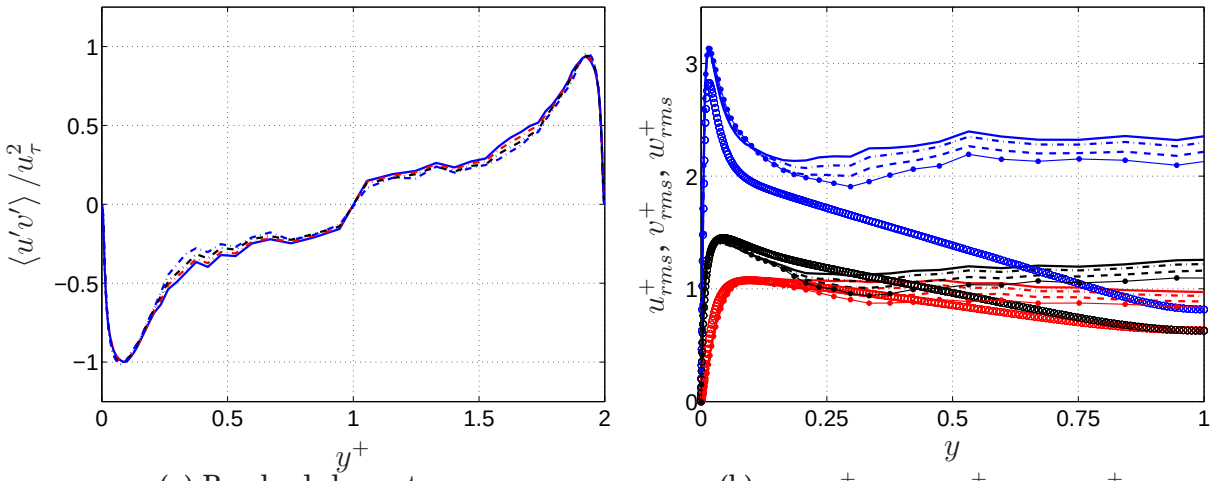

(a) Resolved shear stress.

(b) —: u^+_{rms}; —: v^+_{rms}; —: w^+_{rms}

Figure 5.21: Channel flow using embedded LES. PDH with Δ_{dw}. (a) Time averaged resolved shear stress at $x/\delta = 3.025$. —: $f_{k,int} = 0.025$; - - -: $f_{k,int} = 0.050$; - - -: $f_{k,int} = 0.100$; - - -: $f_{k,int} = 0.200$. (b) Resolved turbulent fluctuations. —: $f_{k,int} = 0.025$; - - -: $f_{k,int} = 0.050$; - - -: $f_{k,int} = 0.100$; - ● -: $f_{k,int} = 0.200$. Markers are DNS data [42]. (Caption only indicates plot symbol for each $f_{k,int}$, colors indicated by figure legend.)

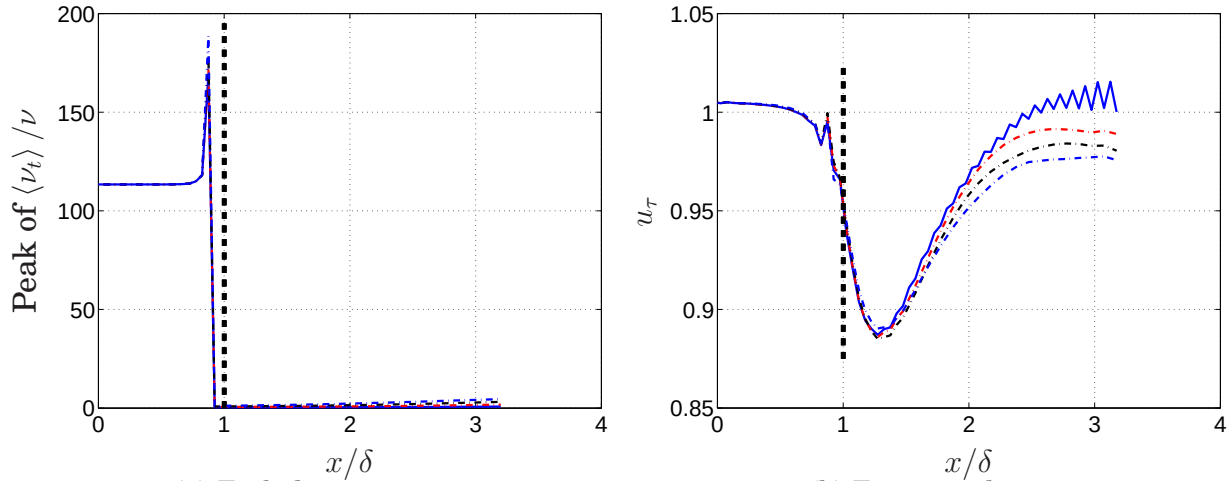

(a) Turbulent viscosity.

(b) Friction velocity.

Figure 5.22: Channel flow using embedded LES. PDH with Δ_{dw}. Time averaged turbulent viscosity and friction velocity. —: $f_{k,int} = 0.025$; - - -: $f_{k,int} = 0.050$; - - -: $f_{k,int} = 0.100$; - - -: $f_{k,int} = 0.200$. Interface indicated by dashed black line.

Further downstream, as the flow develops towards its fully developed LES state, the turbulent viscosity increases (Figure 5.23 (b) and 5.24 (a)) with the subgrid-scale turbulent kinetic energy (not shown). At $x/\delta = 3.025$, the RANS profile is almost recovered and the friction velocity is close to unity, as seen in Figure 5.24

(b). However, the fully developed LES velocity profile, as given by fully developed channel flow (Figure 5.7), is not fully recovered within the extended domain. This is due to the differences in the resolved stresses between the fully developed and the embedded channel flow cases. The resolved turbulent fluctuations at $x/\delta = 6.2250$, as shown in Figure 5.25 (b), indicate a decay of the synthetic turbulence imposed at the interface, especially for $y > 0.1$. Comparison of the resolved turbulent fluctuations at this location to those at $x/\delta = 3.025$ shows that the peak levels of u^+_{rms} are similar, but v^+_{rms} and w^+_{rms} are reduced at $x/\delta = 6.2250$. The peak value of u^+_{rms} corresponds well to that of fully developed channel flow, see Figure 5.9 (a).

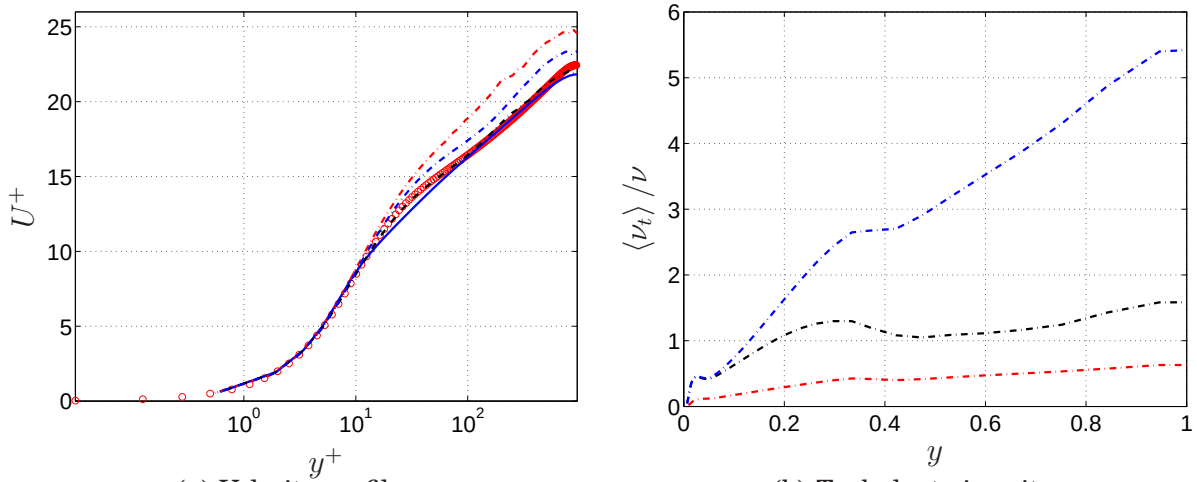

(a) Velocity profiles.

(b) Turbulent viscosity.

Figure 5.23: Channel flow using embedded LES. PDH with Δ_{dw} and $f_{k,int} = 0.050$. Time averaged stream-wise velocity and turbulent viscosity. — : $x/\delta = 0.4250$; - - - : $x/\delta = 1.275$; - - - : $x/\delta = 3.025$; - - - : $x/\delta = 6.2250$. Markers are DNS data [42].

The simulations presented show that the proposed model is well suited for use in an embedded RANS-LES framework. The simulations give overall results that are in good agreement with DNS data and are comparable with other simulations of channel flow using embedded LES, e.g. by Davidson and Peng [6]. The location of the interface relative to the region of interest is important. In the studied flow case, the best results are given at 1.5-2 boundary-layer thicknesses downstream of the RANS-LES interface. Further downstream, the imposed synthetic turbulence decays and the velocity profile starts to diverge from the incoming RANS profile. The value $f_{k,int} = 0.050$ was chosen as optimal for the studied channel flow but has not been tested in any other applications. The generality of $f_{k,int}$ for other flow cases will be investigated in future work. The observed weak model sensitivity to $f_{k,int}$ is however a strength, especially in complex industrial flows, where it is harder to find an optimal value of $f_{k,int}$ than in a well defined academic flow, such as channel flow.

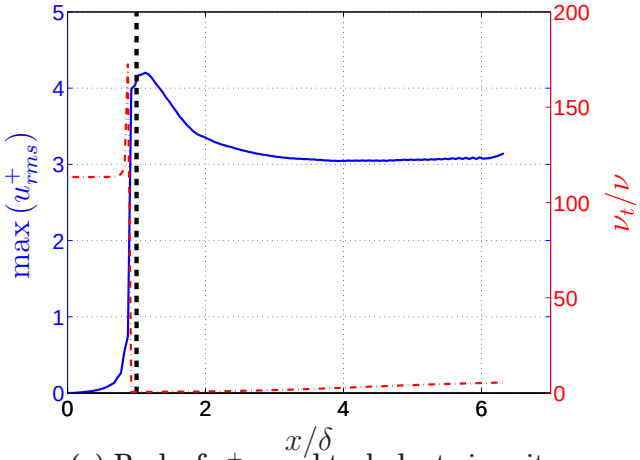

(a) Peak of u^+_{rms} and turbulent viscosity.

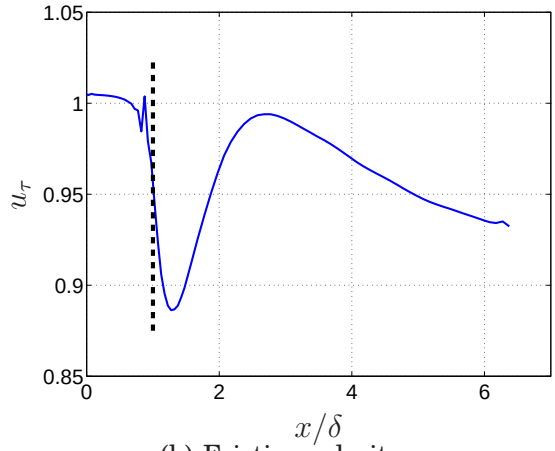

(b) Friction velocity.

Figure 5.24: Channel flow using embedded LES. PDH with Δ_{dw} and $f_{k,int} = 0.050$. (a) Peak of u^+_{rms} and turbulent viscosity. —: peak of u^+_{rms}; - - -: peak of turbulent viscosity. (b) Friction velocity.

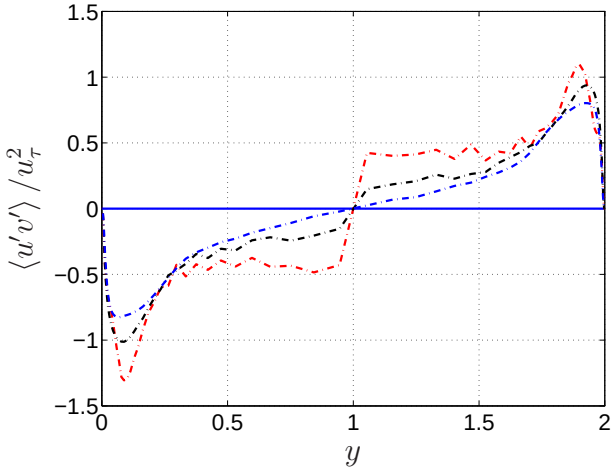

(a) Shear stress.

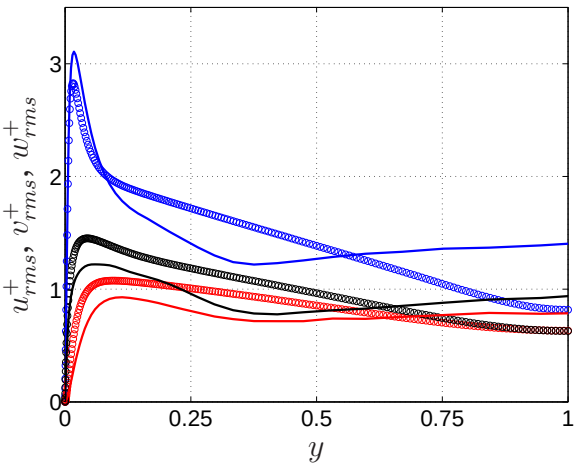

(b) Resolved turbulent fluctuations.

Figure 5.25: Channel flow using embedded LES. PDH with Δ_{dw} and $f_{k,int} = 0.050$. (a) Time averaged resolved shear stress. (a) —: $x/\delta = 0.4250$; - - -: $x/\delta = 1.275$; - - -: $x/\delta = 3.025$; - - -: $x/\delta = 6.2250$. (b) RMS of resolved turbulent fluctuations at $x/\Delta = 6.2250$. —: u^+_{rms}; —: v^+_{rms}; —: w^+_{rms}. Markers are DNS data [42].

Chapter 6

Concluding remarks and future work

6.1 Conclusions

A new hybrid RANS-LES modeling approach, based on the low-Reynolds-number $k-\omega$ model by Peng et al. [11], has been formulated and evaluated in analysis of fundamental turbulent flows. The turbulence-resolving mode incurred in the formulation was calibrated using decaying homogeneous isotropic turbulence and $C_{LES} = 0.70$ was concluded to give the best agreement with experimental data. Through the introduced correction function, Ψ_{PDH}, which aims to cancel the effect of the low-Reynolds-number damping functions in the LES mode, the simulated decay of turbulence, evaluated through energy spectra, shows that the proposed model demonstrates a weak sensitivity to grid refinement. This makes the model versatile and robust, and the C_{LES} parameter does not need to be adapted for different grid resolutions.

The proposed model, in its LES mode, gives improved results compared to the dynamic Smagorinsky and WALE subgrid-scale models in fully developed channel flow at $Re_\tau = 950$. A filter width based on the wall distance was shown to give superior results on the mesh used compared to LES length scales based on more traditional measures, such as the cube root of the control volume or the local maximum cell size. Large differences in the turbulent viscosity produced were observed due to the use of different LES length scales, which affect the turbulence resolving capability.

Using the embedded approach in channel flow at $Re_\tau = 950$, where the upstream part of the channel was modeled with RANS and the downstream domain was treated in LES based on the PDH model, the proposed model gave results in good agreement with DNS data and other comparable studies, e.g. the work of Davidson and Peng [6]. Over the interface, which connects the upstream RANS region with the downstream LES zone, synthetic anisotropic fluctuations were imposed and the RANS properties were scaled to match LES levels. The ratio of subgrid-scale to RANS turbulent kinetic energy, applied at the RANS-LES interface, was $0.025 < f_{k,int} < 0.20$. In this range, the model demonstrated a weak sensitivity to the

interface condition. Only small differences in resolved stresses and velocity profiles were observed in the downstream flow between different interface conditions. This is a preferable behaviour when the model is applied to more complex flows, where adequate interface conditions can be more difficult to define.

In fully developed channel flow at $Re_\tau = 8000$, a zonal hybrid RANS-LES formulation together with a DES formulation of the proposed model were evaluated. Comparative simulations were made with Menter's SST $k-\omega$ model as the base RANS model. In comparison to MSST, the proposed model gives similar or better results on the grid used.

Using the zonal formulation, four different LES length scales were evaluated in order to explore their influence on the log-layer mismatch between the RANS and LES domains. In addition, a variation of location of the RANS-LES interface in the range $250 \leq y^+ \leq 1050$, in the wall normal direction, was done with the purpose of evaluating the model's sensitivity to switch location in combination with the LES length scale and its effect on the log-layer mismatch. The intensity of the mismatch was quantified using the measure of skin friction reduction. The skin friction from the simulations performed was compared to the skin friction estimated via the velocity from the log-law at the channel center line. The well known log-layer mismatch issue in DES simulations was reproduced with PDH and MSST as base models, and the skin friction reduction was in line with previous studies, e.g. the work presented by Nikitin et al. [34].

It was observed that the LES length scale to a large extent influences the intensity of the log-layer mismatch. The wall distance based LES length scale showed also here improved performance compared to e.g. Δ_{max} and Δ_{vol}. The main explanation for the success of the wall distance based LES length scale is the quick reduction of the turbulent viscosity, and in turn the subgrid-scale turbulent kinetic energy, across the RANS-LES interface. This was observed especially for the interfaces located at $y^+ = 250$ and 520. The effect of such a quick reduction is that the turbulence-resolving flow is already well developed at the interface. In comparison with the length-scale formulations based on the local maximum cell size, the cell volume or the vorticity, where the reduction of the turbulent viscosity is much slower across the interface, the modeled stresses dominate in the interface region, which enhances the log-layer mismatch and hence the over-prediction of the velocity.

The discrepancies between the classical filter width based on the maximum local cell size and the filter width based wall distance were increased when the RANS-LES interface was moved closer to the wall. Since the differences between these LES length scales increase when the wall is approached, the results meet the expectations and confirm the importance of a well suited turbulent viscosity level at the interface to reduce the log-layer mismatch.

6.2 Future work

The work presented in this thesis should be seen as the first step towards a versatile and robust turbulence-resolving model based on the PDH LRN $k-\omega$ model. So far, the proposed model has only been applied to fully developed channel flow and channel flow using embedded LES. To gain further confidence, it must be applied to other kinds of flows, where e.g. large recirculations and free-shear layers are present. The zonal and embedded formulations presented in this work have shown promising performance and are good candidates for more advanced applications, such as the transonic duct flow case [10].

To achieve a more versatile model, suitable for industrial needs, the challenge consists of performing a safe treatment of boundary layers and making wall-modeled LES available. The first issue, safe treatment of boundary layers, is important for external aerodynamics where attached boundary layers are often present in combination with massively separated flows, e.g. cavities and wake flow behind bluff bodies. Other applications where a safe treatment of boundary layers come into play are e.g. buffeting and shock-induced boundary-layer separation. The second issue, wall-modeled LES, is indeed important in applications such as inlet air ducts, where shallow separations often occur and the boundary layer turbulence is essential for predicting aircraft engine stability.

Zonal formulations tend to put a heavy load on the user, since RANS and LES zones have to be specified manually and the user must have good knowledge of the flow to place these regions in a suitable way. Global methods, such as DDES and IDDES, do not need any input from the user, as regards zonal partitioning. Thus, this strategy is better suited for flows involving complex geometries and hence this experience should be put into the proposed hybrid RANS-LES modeling approach.

The continuation of this study will further explore the proposed model in a global method perspective as well as in an embedded/zonal perspective. The focus should be on the search for suitable RANS-LES switching criteria in global type formulations to increase the applicability to aeronautical needs. The issue of the grey area needs to be further highlighted to reach greater accuracy in predictions of free shear layers and to reduce the log-layer mismatch. Considering a zonal/embedded approach, the proposed model has been shown to perform well in embedded channel flow. However, flows with more arbitrary RANS-LES interfaces should be studied in order to gain greater confidence in the interface conditions.

It is important to take into consideration that the simulations performed with the proposed model have been made using a block structural code and with meshes of high quality. In industrial applications, the meshes are mostly unstructured, and no specific grid line can be used as the RANS-LES interface, as in the presented zonal/embedded approach. In unstructured meshes, prismatic layers are commonly used to resolve the boundary layers, and tetrahedrals are used to capture the off-wall flow. Moreover, grids designed for turbulence-resolving flow should be homogeneous in the off-wall regions, i.e either cubic cells should be used in structured grids or tetrahedral cells in unstructured grids (other polyhedral elements can be used as

long as they are not stretched). For homogeneous grids and away from the wall, there is no difference between the evaluated LES length scales (Δ_{dw}, Δ_{max}, Δ_{vol} and Δ_{ω}). However, in the boundary layer, which is resolved with prismatic layers, the different length scales will justify their purpose. Unfortunately, the outer boundary layer cannot always be simulated using prismatic layers, due to computational costs and/or geometrical constraints, but has to be predicted within the tetrahedral mesh. These issues and their effect on the accuracy of the model are important and should be further analyzed in an extension of the proposed model to unstructured grids and solvers.

Bibliography

[1] Girimaji S. Partiall-Averaged Navier-Stokes model for turbulence: a Reynolds-averaged Navier-Stokes to direct numerical simulation bridging method. *Journal of Fluids Engineering*, 73:413–421, 2006.

[2] Chaouat B. and Schiestel R. A new integrated transport model for subgrid-scale stresses and dissipation rate for turbulent developing flows. *Physics of Fluids*, 17, 2005.

[3] Menter F.R. and Ergorov Y. The scale-adaptive simulation method for unsteady turbulent flow predictions. part 1: Theory and model description. *Flow, Turbulence and Combustion*, 85:113–138, 2010.

[4] Basara B., Krajnović S., Girimaji S., and Pavlović Z. Near-wall formulation of the Partially Averaged Navier Stokes turbulence model. *AIAA Journal*, 49:2627–2636, 2011.

[5] Ma J.M, Peng S.-H., Davidson L., and Wang F.J. A low Reynolds number variant of partially-averaged Navier-Stokes model for turbulence. *International Journal of Heat and Fluid Flow*, 32:652–669, 2011.

[6] Davidson L. and Peng S-H. Embedded Large-Eddy Simulation Applied to Channel Flow and Hump Flow. *AIAA Journal, accepted and to be published*, 2013.

[7] Davidson L. A New Approach of Zonal Hybrid RANS-LES Based on a Two-Equation $k-\omega$ Model. ETMM9, Thessaloniki, 6-8 June 2012, 2012.

[8] Spalart P.R. and Allmaras S.R. A one-equation turbulence model for aerodynamic flows. *La Recherche Aérospatiale, 1, p. 5-21*, 1:5–21, 1994.

[9] Menter F. R. Two-equation eddy-viscosity turbulence models for engineering applications. *AIAA Journal*, 32:1598–1605, 1994.

[10] Arvidson S., Peng S-H., and Davidson L. Feasibility of hybrid RANS-LES of shock/boundary-layer interaction in a duct. In Fu S. et al., editor, *Progress in Hybrid RANS-LES Modelling*, volume 117 of *NNFM*. Springer, 2012.

[11] Peng S-H., Davidson L., and Holmberg S. A Modified Low-Reynolds-Number $k-\omega$ Model for Recirculating Flows. *Journal of Fluids Engineering*, 119:867–875, 1997.

[12] Yan J., Mockett C., and Thiele F. Investigation of alternative length scale substitutions in detached-eddy simulation. *Flow, Turbulence and Combustion*, 74:85–102, 2005.

[13] Wilcox C.W. Reassessment of the scale-determinig equation for advanced turbulence models. *AIAA Journal*, 26:1299–1310, 1988.

[14] Smagorinsky J. General circulation experiments with the primitive equations. *Monthly Weather Review*, 91:99–165, 1963.

[15] Kok J.C. and van der Ven H. Capturing free shear layers in hybrid RANS-LES simulations of separated flow. Second Symposium "Simulation of Wing and Nacelle Stall" 21st-22nd June 2012, Braunschweig, Germany, 2012.

[16] Ashton N., Prosser R., and Revell A. A hybrid numerical scheme for a new formulation of delayed detached-eddy simulation (DDES) based on elliptic relaxation. *Journal of Physics: Conference Series*, 318:1–14, 2011.

[17] Spalart P., Jou W-H., Strelets M., and Allmaras S. R. Comments on the feasability of les for wings, and on a hybrid rans/les approach. In *Advances in DNS/LES*, Ruston, Lousiana, 1997.

[18] Spalart P.R. Detached-eddy simulation. *Annual Review of Fluid Mechanics*, 41:181–202, 2009.

[19] Strelets M. Detached eddy simulation of massively separated flows. AIAA 2001-0879, Reno, Nevada, 2001.

[20] Kok J., Dol H.S., Oskam B., and van der Ven H. Extra-large simulation of massivlley separated flows. AIAA 2004-0264, Reno, Nevada, 2004.

[21] Kok J.C. Resolving the dependence on freestream values for the $k-\omega$ turbulence model. *AIAA Journal*, 38:1292–1295, 2000.

[22] Menter F.R, Kuntz M., and Langtry R. Ten years of industrial experience with the sst turbulence model. *Turblence, Heat and Mass Transfer*, 4, 2003.

[23] Spalart P.R., Deck S., Shur M.L., Squires K.D., Strelets M. Kh., and Travin A. A new version of detached-eddy simulation, resistant to ambiguous grid densities. *Theory of Computational Fluid Dynamics*, 20:181–195, 2006.

[24] Deck S. Zonal-Detached-Eddy Simualtion of the Flow Around a High-Lift Configuration. *AIAA Journal*, 43:2372–2384, 2005.

[25] Deck S. Recent improvments in the zonal detached eddy simualtion (ZDES) formulation. *Theoretical and Computational Fluid Dynamics*, 2011.

[26] Davidson L. and Peng S-H. Hybrid LES-RANS modelling: a one-equation SGS model combined with a $k-\omega$ model for predicting recirculating flows. *International Journal for Numerical Methods in Fluids*, 43:1003–1018, 2003.

[27] L. Davidson and M. Billson. Hybrid LES/RANS Using Synthesized Turbulence for Forcing at the Interface. *International Journal of Heat and Fluid Flow*, 27(6):1028–1042, 2006.

[28] Davidson L. and Dahlström S. Hybrid RANS-LES: an Approach to make LES Applicable at High Reynolds Number. *International Journal of Computational Fluid Dynamics*, 19(6):415–427, 2005.

[29] Chauvet N., Deck S., and Jaquin L. Zonal Detached Eddy Simualtion of a Controlled Propulsive Jet. *AIAA Journal*, 45:2458–2473, 2007.

[30] Shur K.L., Spalart P.R., Strelets M.Kh., and Travin A.K. A hybrid RANS-LES approach with delayed-DES and wall-modelled LES capabilities. *International Journal of Heat and Fluid Flow*, 29:1638–1649, 2008.

[31] Gritskevich M.S., Garbaruk A.V., Schütze J., and Menter F. Development of DDES and IDDES Formulations for the $k - \omega$ Shear Stress Transport Model. *Flow, Turbulence and Combustion*, 88:431–449, 2012.

[32] Breuer M., Joicic N., and Mazaev K. Comparison of DES, RANS and LES for the separated flow around a flat plate at high incidence. *International Journal for Numerical Methods in Fluids*, 41:357–388, 2003.

[33] Spalart P.R. Young-person's guide to detached-eddy simulation grids. NASA CR-2001-211032, 2001.

[34] Nikitin N.V., Nicoud F., Wasistho B., Squires K.D., and Spalart P.R. An approach to wall modeling in large-eddy simulations. *Physics of Fluids*, 12:1629–1632, 2000.

[35] Davidson L. and Dahlström S. Hybrid LES-RANS: An approach to make les applicable at high reynolds number. *International Journal of Computational Fluid Dynamics*, 19:415–427, 2007.

[36] Emvin P. *The full multigrid method applied to turbulent flow in ventilated enclosures using structured and unstructured grids*. PhD thesis, Chalmers University of Technology, 1997.

[37] Eliasson P. EDGE, a Navier-Stokes Slover for Unstructured Grids. Scientific report FOI-R-0298-SE, Computational Aerodynamics Department, Aeronautics Division, FOI, 2001.

[38] Wilcox C. W. Simulation of Transition with a Two-Equation Turbulence Model. *AIAA Journal*, 32:247–255, 1994.

[39] Mocket C. *A comprehensive study of detached-eddy simulation*. PhD thesis, der Technischen Universität Berlin, 2009.

[40] Comte-Bellot G. and Corrsin S. Simple Eularian time correlation of full- and narrow-band velocity signals in grid-generated “isotropic” turbulence. *Journal of Fluid Mechanics*, 48(2):273–337, 1971.

[41] Bunge U., Mockett C., and Thiele F. Calibration of different models in the context of detached-eddy simulation. Arbetisgemeinschaft ”Strömmungen mit Ablösung” STAB Jahersbericht, 2003.

[42] Hoyas S. and Jimenez J. Reynolds number effects on the reynolds-stress budgets in turbulent channels. *Physics of Fluids A*, 20:101511, 2008.

[43] Germano M., Piomelli U., Moin P., and Cabot W.H. A dymanic subgridscale eddy viscosity model. *Physics of Fluids A*, 3:1760–1765, 1991.

[44] Nicoud F. and Ducros F. Subgrid-Scale Stress Modelling Based on the Square of the Velocity Gradient Tensor. *Flow, Turbulence and Combustion*, 62:183–200, 1999.